AD-A065 181 LOCKHEED-GEORGIA CO MARIETTA F/G 20/4
DEVELOPMENT OF A VISCOUS VORTEX/WING INTERACTION PROGRAM FOR TH--ETC(U)
NOV 78 C J DIXON, S SAMPATH N00014-74-C-0151
UNCLASSIFIED L678ER0227 ONR-CR215-233-4F NL

| OF |
ADA
065181

END
DATE FILMED
4-79
DDC

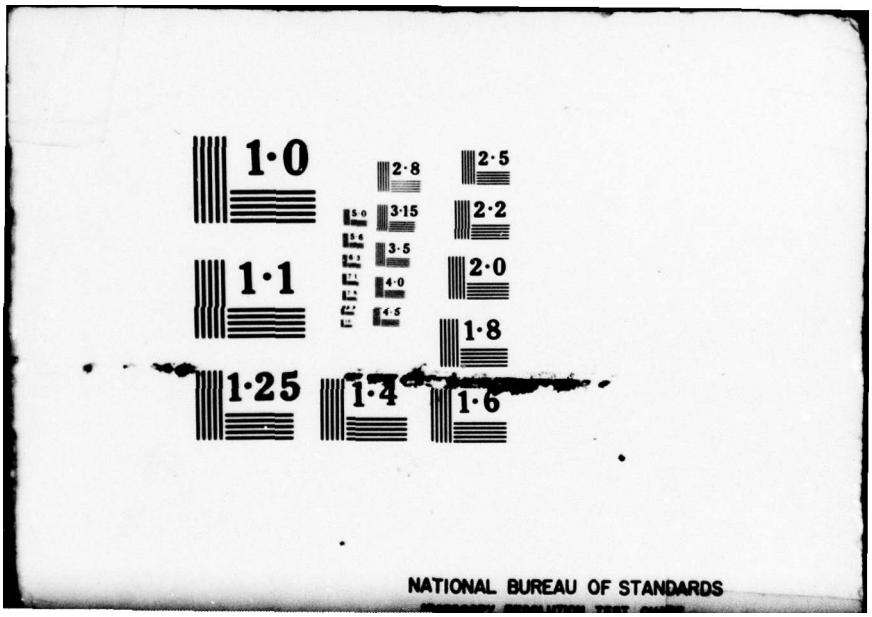
1·0
1·1
1·25
2·8
3·15
3·5
4·0
4·5
1·4
2·5
2·2
2·0
1·8
1·6
NATIONAL BUREAU OF STANDARDS

LEVEL II

REPORT ONR-CR-215-233-4F

(12)

AD A065181

DDC FILE COPY

DEVELOPMENT OF A VISCOUS VORTEX/WING INTERACTION PROGRAM FOR THICK WINGS WITH ROUNDED LEADING EDGE

CHARLES J. DIXON
Lockheed-Georgia Company
Marietta, Georgia

S. SAMPATH
Consultant
Lockheed-Georgia Company
Marietta, Georgia

DDC
RECEIVED
MAR 2 1979
A

CONTRACT N00014-74-C-0151
ONR TASK 215-233

NOVEMBER 1978

FINAL REPORT

Approved for public release; distribution unlimited.

PREPARED FOR THE

OFFICE OF NAVAL RESEARCH ● 800 N. QUINCY ST. ● ARLINGTON ● VA ● 22217

79 03 01 001

Change of Address

Organizations receiving reports on the initial distribution list should confirm correct address. This list is located at the end of the report. Any change of address or distribution should be conveyed to the Office of Naval Research, Code 211, Arlington, VA 22217.

Disposition

When this report is no longer needed, it may be transmitted to other organizations. Do not return it to the originator or the monitoring office.

Disclaimer

The findings and conclusions contained in this report are not to be construed as an official Department of Defense or Military Department position unless so designated by other official documents.

Reproduction

Reproduction in whole or in part is permitted for any purpose of the United States Government.

UNCLASSIFIED

SECURITY CLASSIFICATION OF THIS PAGE (When Data Entered)

(19) **REPORT DOCUMENTATION PAGE**

READ INSTRUCTIONS BEFORE COMPLETING FORM

1. REPORT NUMBER: (18) ONR CR215-233-4F
2. GOVT ACCESSION NO.
3. RECIPIENT'S CATALOG NUMBER

4. TITLE (and Subtitle): (6) DEVELOPMENT OF A VISCOUS VORTEX/WING INTERACTION PROGRAM FOR THICK WINGS WITH ROUNDED LEADING EDGE,
5. TYPE OF REPORT & PERIOD COVERED: (9) Final Report,
6. PERFORMING ORG. REPORT NUMBER: (14) LG78ER0227

7. AUTHOR(s): (10) Charles a J. Dixon, S. Sampath
8. CONTRACT OR GRANT NUMBER(s): (15) N00014-74-C-0151

9. PERFORMING ORGANIZATION NAME AND ADDRESS
Lockheed-Georgia Company
Marietta, Georgia 30063
10. PROGRAM ELEMENT, PROJECT, TASK AREA & WORK UNIT NUMBERS
61153N
RR014-11-84

11. CONTROLLING OFFICE NAME AND ADDRESS
Office of Naval Research
Vehicle Technology Program, Code 211
800 N. Quincy Street, Arlington, Va. 22217
12. REPORT DATE: (11) 30 November 1978
13. NUMBER OF PAGES: (12) 93 p.

14. MONITORING AGENCY NAME & ADDRESS (if different from Controlling Office): (16) RR0 1411
15. SECURITY CLASS. (of this report): Unclassified
15a. DECLASSIFICATION/DOWNGRADING SCHEDULE

16. DISTRIBUTION STATEMENT (of this Report)
Approved for public release; distribution unlimited.
(17) RR0 141184

17. DISTRIBUTION STATEMENT (of the abstract entered in Block 20, if different from Report)

18. SUPPLEMENTARY NOTES

19. KEY WORDS (Continue on reverse side if necessary and identify by block number)
Vortex Lift, vortex control, viscous mixing, Navier-Stokes, computational fluid mechanics, delta wings, high angle of attack, 3-D boundary layer, vorticity, flow separation

20. ABSTRACT (Continue on reverse side if necessary and identify by block number)
A hybrid viscous/potential flow program ~~has been~~ was developed to analyze the flow field on and around a swept thick wing with rounded leading edges and leading edge vortex flow. The program developed for this report provides a computational package which includes four major programs run with proper interfacing in an iterative cycle. These programs include two viscous programs and two potential flow programs. The viscous flow programs consist of: (1) a

(Continued on reverse)

DD FORM 1 JAN 73 1473 EDITION OF 1 NOV 65 IS OBSOLETE

UNCLASSIFIED

SECURITY CLASSIFICATION OF THIS PAGE (When Data Entered)

210065 79 03 01 001

20. Abstract (continued)

parabolic solution to the Navier-Stokes vorticity equation in a box around the leading edge vortex; and (2) a three-dimensional second-order boundary layer program for infinite yawed wings. This program provides the boundary layer vorticity being fed into the vortex box. The two potential flow programs are (1) the Hess surface singularity method for thick wings and fuselage combination and (2) a vortex lattice method to model the leading edge vortex. These two programs provide the surface pressures and the viscous box boundary velocities.

The program interfaces are developed by applying the concept to a 65 deg delta wing with a spanwise variation in leading edge radius. Operating experience is presented, in the report, giving the results and knowledge gained in each cycle of the iterations. Results of these investigations show the feasibility of the concept and provide insight to some of the critical parameters. With further application experience, the program has the capability of being developed into a design tool that will take advantage of the leading edge vortex to improve the economy, performance and flying qualities of future aircraft in the takeoff, landing and maneuvering modes. Specifically, the method allows the designer to design or modify the leading edge shape to meet the desired performance and control requirements.

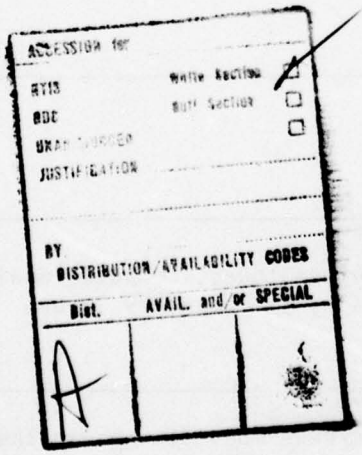

SUMMARY

The current interest in aircraft exhibiting leading edge vortex flows during takeoff, landing, and high angle maneuver has led to the computational method development discussed in this report. These methods are directed to the analysis of the forces and flow field around arbitrary swept wing planforms having thick airfoils with rounded leading edges and leading edge vortex flow. Due to the nature of this type of flow field viscous effects must be considered in the method. These are not feasible to obtain by solving the Navier-Stokes equations for the entire flow field. Therefore, in contrast to other known empirical, potential flow methods, the method discussed herein provides an optimum combination of viscous and potential flow models. This combination is developed with three goals in mind. One is to maintain minimum computer time, yet still provide insight into the mechanisms of the flow field. The second is for the solutions to be valid for large-scale configurations, i.e. without Reynolds number limitations. The third goal is to provide a design tool which by optimizing leading edge shape takes advantage of the leading edge vortex in improving the economy, performance and flying qualities of future aircraft.

The method described herein is a computational package which includes four major programs run with proper interfacing in an iterative cycle. These programs are: (1) a viscous program which solves parabolized Navier-Stokes equations within a box containing the vortex flow on the upper wing surface, (2) a three-dimensional, second-order boundary layer program which provides the strength and distribution of the leading edge vorticity being fed into the viscous box, (3) a potential flow program which models the three-dimensional thick wing using the Hess surface singularity method, and (4) a potential influence vortex program to model the leading edge vortex system. The two potential flow programs provide both the pressure coefficients required for the boundary layer program and the velocity boundary conditions for the viscous box. The viscous box provides not only the primary vortex, but other viscous effects such as the vortex core velocities and the secondary vortex.

To develop the interfacing and convergence techniques of these four programs, an application was made to a 65° delta wing with spanwise variation in leading edge radius. Operating experience is presented in this report. Each cycle through all the programs has contributed not only to the operating techniques for interfacing the programs, but to a knowledge of the critical parameters. It is shown in this report that aircraft loads and moments can be critically dependent on the strength and distribution of the vorticity shed from the wing leading edge into the primary vortex. This vorticity is dependent on local angle of attack, leading edge shape, Reynolds number, and the boundary layer state (laminar or turbulent).

Several trial runs have been made exercising all program elements sequentially to develop effective interface and convergence techniques. Finally, these techniques are employed in a case where three consistent cycles of the full program are completed to evaluate the extent of solution convergence. This case suggests additional convergence techniques while demonstrating the feasibility of the overall method and providing direction for future work.

Recommendations presented for future efforts lie in two categories. One concerns program changes to make the method more versatile and accurate. The other reflects on the need for both additional operational experience with the current program and experimental verification of some of the resulting flow field parameters.

PREFACE

The research described in this report was performed under Contract No. N00014-74-C-0151 for the Office of Naval Research. Dr. R. E. Whithead of the Vehicle Technology Program served as ONR Contract Monitor, while C. J. Dixon of Lockheed-Georgia's Advanced Flight Sciences Department served as program manager. Dr. S. Sampath of Lockheed and Drs. R. M. Scruggs and J. F. Nash of Sybucon, Inc. made significant contributions to the computational development. Computer time was contributed by NASA-Ames Aircraft Aerodynamic Branch.

CONTENTS

	Page
SUMMARY	3
PREFACE	5
TABLE OF CONTENTS	7
LIST OF FIGURES	9
LIST OF SYMBOLS	11
1.0 INTRODUCTION	13
2.0 SOLUTION PROCEDURE	16
3.0 POTENTIAL FLOW MODELS	22
3.1 Vortex Lattice Program	22
3.2 Thick Wing Potential Flow Model	24
3.3 Integration of Vortex Lattice Model and AIP Program	25
4.0 BOUNDARY LAYER PROGRAM	31
4.1 Requirement for Leading Edge Vorticity	31
4.2 Second-Order Boundary Layer Method	33
4.3 Boundary Layer Results	35
4.4 Application of Boundary Layer Program	45
5.0 VISCOUS BOX CALCULATIONS	48
5.1 Governing Equations	48
5.2 Initial and Boundary Conditions	49
5.3 Modifications to Finite Difference Technique	50
5.4 Reconstruction of Free Vortex Geometry	52
6.0 PROGRAM INTERFACING AND SAMPLE CALCULATIONS	53
6.1 Model Description	54
6.2 Results of First Three Cases of Investigations	56
6.3 Case 4 - Incorporation of Program Corrections Developed in Cases 1 through 3	75
7.0 APPLICATIONS	84
8.0 CONCLUSIONS	87
9.0 RECOMMENDATIONS FOR FURTHER EFFORT	88
REFERENCES	90

PRECEDING PAGE BLANK-NOT FILMED

LIST OF FIGURES

Figure		Page
2.1	Viscous Box Positions on 65° Wing	17
2.2	Airfoil/Viscous Box Relation	18
2.3	Computational Flow Chart	19
3.1	Free Vortex System Showing One Typical Element	23
3.2	Panels for C-5A Wing/Fuselage/Empennage	26
3.3	Pressure Distributions for C-5A Wing at 36.9% Span	27
3.4	Potential Flow Integration Program	29
3.5	Conventional Panelling	30
3.6	Conical Panelling	30
4.1	Section Showing Boundary Layer First and Second-Order Domains	32
4.2	Wing Section Showing Boundary Region Coordinate System	32
4.3	Boundary Layer Iterative Procedure	36
4.4	Stagnation Line Flow - Infinite Yawed Cylinder	37
4.5	Upper Surface Boundary Layer for Box 2 Face	38
4.6	Boundary Layer Profile Near Flow Separation	39
4.7	Boundary Layer Program Test Model, $\Lambda = 22°$	41
4.8	Boundary Layer Thickness for 22° Wing	42
4.9	Boundary Layer Profiles Near Separation, $\Lambda = 22°$ Wing	44
5.1	Effect of Differencing Scheme on the Diffusion of a Lamb Vortex	51
6.1	Streamwise Section Leading Edge Shape	55
6.2	Viscous Box Relation to Airfoil on 65° Wing - Box 2 Face	57
6.3	Viscous Box Relation to Airfoil on 65° Wing - Box 3 Face	58

PRECEDING PAGE BLANK-NOT FILMED

Figure		Page
6.4	Viscous Box Relation to Airfoil on 65° Wing – Box 4 Face	59
6.5	Viscous Box Relation to Airfoil on 65° Wing – Box 4 End	60
6.6	Free Vortex Vertical Position – Cases 1 and 2	61
6.7	Free Vortex Spanwise Position – Case 2	62
6.8	Free Vortex Strength – Case 1	63
6.9	Spanwise Boundary Layer Circulation – Case 1	65
6.10	Spanwise Boundary Layer Circulation – Case 3	68
6.11	Free Vortex Vertical Position – Cases 2 and 3	69
6.12	Free Vortex Spanwise Position – Cases 2 and 3	70
6.13	Free Vortex Strength – Cases 2 and 3	71
6.14	Cross-Flow Velocity at Free Vortex – Case 1	74
6.15	Boundary Layer Input to Viscous Box	77
6.16	Vortex Strength Output from Viscous Box	78
6.17	Boundary Layer Vorticity Convection Direction	80
6.18	Free Vortex Position, Case 4	81
6.19	Flow Field Velocity Vectors, Case 4, Cycle 3	83
6.20	Flow Field Vorticity Vectors, Case 4, Cycle 3	83

SYMBOLS

C_L	Lift coefficient
C_M	Pitching moment
C_p	Pressure coefficient
C_R	Wing root chord
C	Momentum coefficient for spanwise blowing
M	Mach number
N	Direction normal to surface
P	Pressure
R	Radius of free vortex
R_e, R_N	Reynolds number
S	Distance along stream tube in boundary layer
U, V, W	velocities in x, y, z direction, respectively
U	local edge velocity of boundary layer
$V_\perp$	component of free stream normal to wing leading edge
Y_p	distance normal to wing leading edge
x, y, z	rectangular coordinates - depends on program. See Figure 2.1 for Hess program dnd viscous box. See Figure 4.2 for boundary layer.
X_B	intersection of box plane with root chord
Γ	circulation
δ	boundary layer thickness
ε	angle between box no-slip surface and airfoil chord
α	wing angle of attack
ρ	density and radius of airfoil leading edge
ν	kinematic viscosity
ϕ	parameter defining differencing technique

Λ	wing sweep
η	fraction of spanwise position and vorticity normal to viscous box x-z plane
θ	slope of airfoil
ξ	vorticity normal to y-z plane of viscous box
ζ	vorticity normal to x-y plane of viscous box
ω	total vorticity

Subscripts

v	related to free vortex
t	wing thickness

1.0 INTRODUCTION

The favorable lifting effects of leading edge vortices on delta wings have been under investigation for many years. Several years ago the TFX configurations resulting in the F111 found favorable effects of the leading edge "strake" effect on maximum lift coefficients. The F116, F14 and other fighter type of aircraft have more recently taken advantage of vortex lift. Latest application of vortex lift is found in the "Space Shuttle" configuration and the supersonic "Concorde". Future supersonic configurations will be aided or plagued by the effects of leading edge vortex formation depending on the point of view or application thereof. Vortex flow contains considerable energy which most often shows up as drag; however, the current direction is to use vortex flow to improve lift. The question remaining is, "Can L/D also be improved when designing for vortex lift?". For many cases the leading edge vortex is persistent regardless of attempts to eliminate it; therefore, it must be put to useful work.

There have been many attempts to model the flow for delta wings with leading edge vortices. Matoi[1] has provided a good survey of many of these attempts. The efforts of most have been limited to potential flow models, assuming rotational elements for viscous effects such as the leading edge feeding sheet. The basic assumption of slender-body, conical flow have been followed by most investigators such as Mangler and Smith[2]. Results of these early investigators have laid a good foundation for further research, but they are not successful in obtaining forces, and moments over a general range of configurations. Polhamus[3] and Lamar[4] have had good success in predicting vortex lift with the leading edge suction analogy for sharp edge wings. This method, however, does not describe the pressures or flow mechanism. Good results were obtained most recently by Weber, et al.[5] and Rao and Nathnan[6], where the trailing edge conditions of delta wings are included in the boundary conditions. Kandil[7] has also provided a good potential flow model and convergence criteria. Currently these programs appear to have limits that restrain their application to certain configurations. These limits are as follows:

(1) Thin wings only are considered.

(2) Starting conditions at leading edge must be assumed.

(3) The viscous condition of no slip at the wing surface in the area of the free vortex is not satisfied and this can affect final vortex position and strength.

(4) No secondary vortex system is included.

(5) Vortex burst cannot be predicted.

Based on verbal comments from others involved in this field, some of the above investigators are beginning to apply the necessary viscous tools to remove the above limitations. G. F. Hall, et al.[8] have recognized the need to combine viscous solutions with potential flow techniques for application to the formation of a tip vortex from a semi-infinite wing. Their methods are similar to those employed by Lockheed. Lockheed-Georgia Company has been developing the necessary viscous tools for approximately three years under Office of Naval Research contract and now has integrated the computer programs that have the potential to remove practically all of the above limitations. The fifth limitation, vortex bursting, is not well resolved, but the methods do give indication of incipient burst. Some empirical work must still be applied to this prediction. The resulting hybrid viscous/potential flow program is intended to provide the flow field velocities, pressures and forces for arbitrary configurations having interfering vortex/wing flows. Thick rounded leading edge wings with leading edge vortex due to flow separation from the swept leading edges can be analyzed. This hybrid program combines two elliptic potential flow programs, a "viscous box" Navier-Stokes solution containing the vortex and a boundary layer program.

The original effort to develop the "viscous box" technique is reported in references 9 and 10. These reports were primarily concerned with leading edge vortex control by spanwise blowing, SWB. Application was limited to straight or moderately swept wings since the box boundary conditions and flow-field velocities were obtained by a Green's function

integral technique. Later the interest turned to highly swept wings without SWB. This required a more accurate technique to supply the boundary conditions to the viscous box. Reference 11 reports the development of the hybrid viscous box/elliptical potential flow vortex lattice method as applied to thin sharp edged delta wings. In this technique the elliptic vortex lattice program, through iteration, supplied the box boundary velocities, but the vorticity shed from the leading edge across the box boundary still had to be empirically estimated. A sensitivity study showed the strength and direction of this feeding vorticity to be very critical to the overall solution. This led to the development of a boundary layer program to supply this need. With this additional tool, thick rounded leading edge wings with leading edge separation can be treated as well as thin wings if joined with a thick wing potential flow model and the viscous box concept. The development and integration of these tools for the thick wing is the subject of this report.

2. SOLUTION PROCEDURE

The computational package includes four major programs which are run with proper interfacing in an iterative cycle. The coordinate system for these programs and the regions where they are used are indicated in figure 2.1 and 2.2. The flow chart of figure 2.3 shows the sequence of computations using these programs. The capabilities of individual programs are described in subsequent chapters; the overall computational sequence and the interfacing computational work between the major calculations are described below.

The major programs employed in the computations are: (1) Aircraft Interference Program (AIP), which models the three-dimensional thick wing using potential flow assumption, (2) a vortex lattice program to model the leading edge vortex system for the delta wing, (3) a three-dimensional, second-order, boundary layer program, and (4) a viscous box program that solves parabolized Navier-Stokes equations on the upper surface of the delta wing. The potential flow models provide the pressure coefficients required for the boundary layer calculation in addition to the velocity boundary conditions for the viscous box calculations. The step-by-step procedure given below supplements the flow chart of figure 2.3.

(1) Define coordinates of panels on the wing for AIP program. Determine the centroids of these panels which form the control points for AIP program.

(2) Define control points for the vortex lattice program. An optimum choice of panelling procedure for these two steps is described in Section 3.

(3) Define in global coordinates, for AIP program, the coordinates of grid points on the box boundaries.

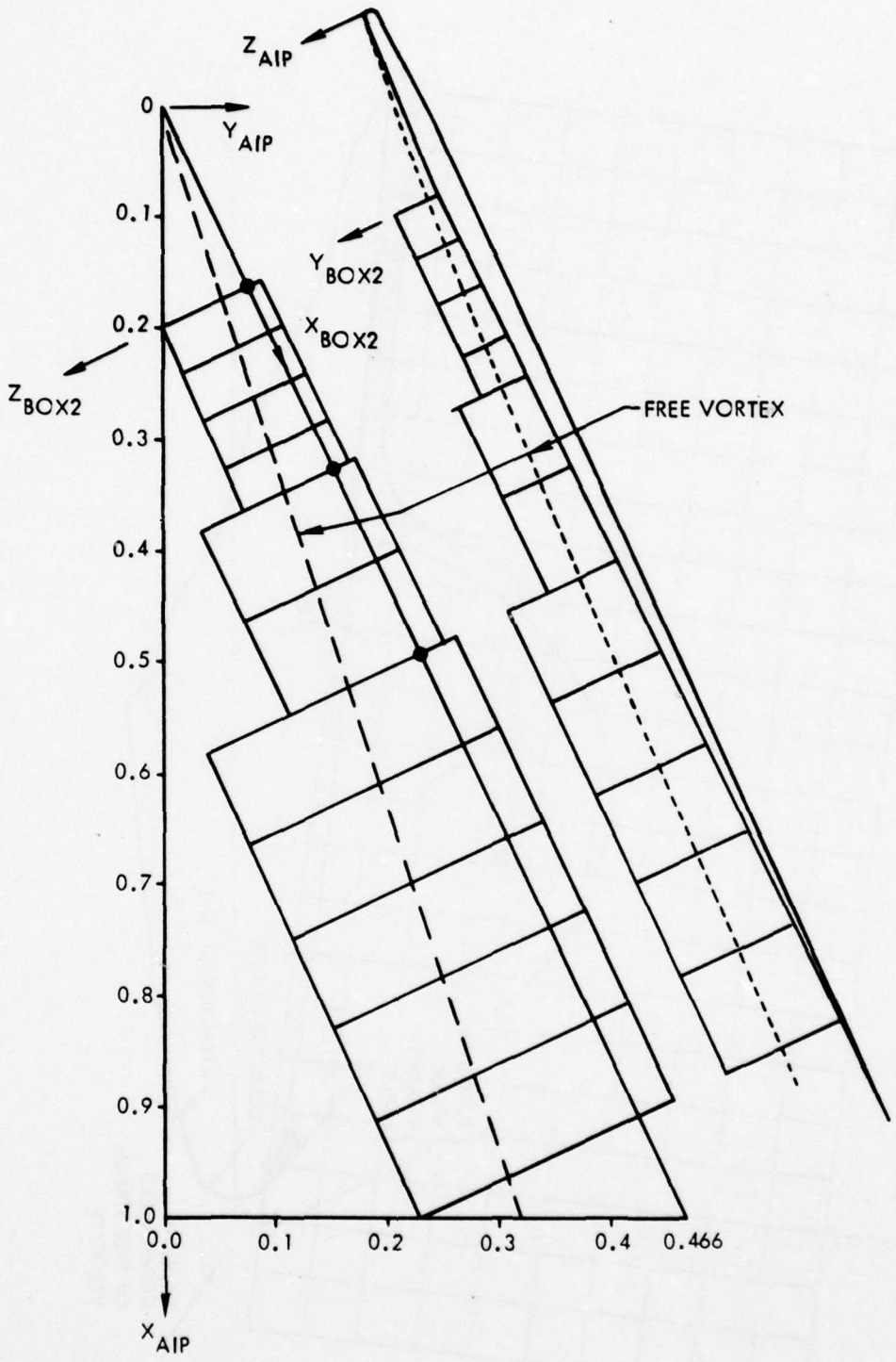

Figure 2.1. Viscous Box Positions on 65° Wing

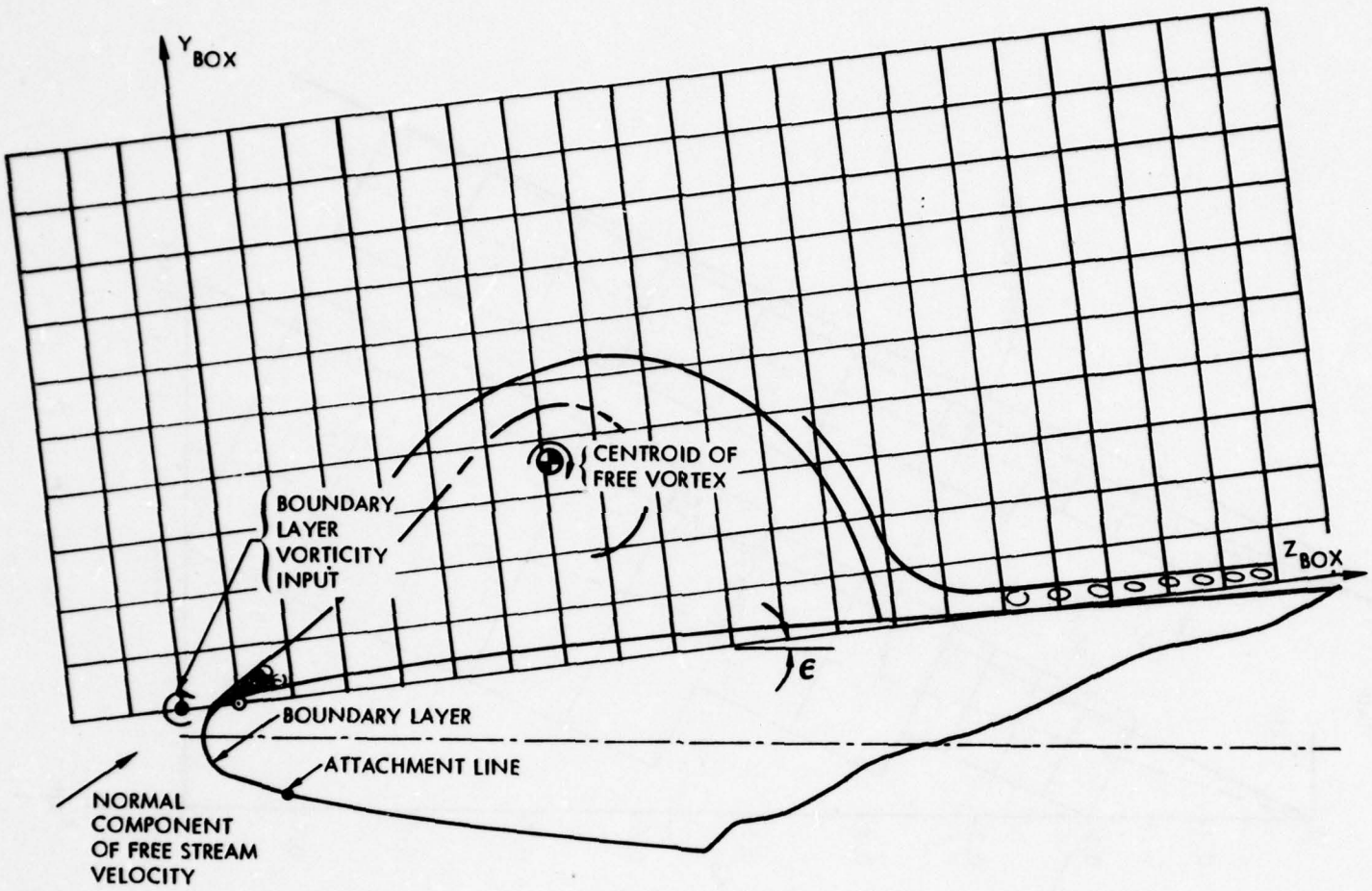

Figure 2.2. Airfoil/Viscous Box Relation

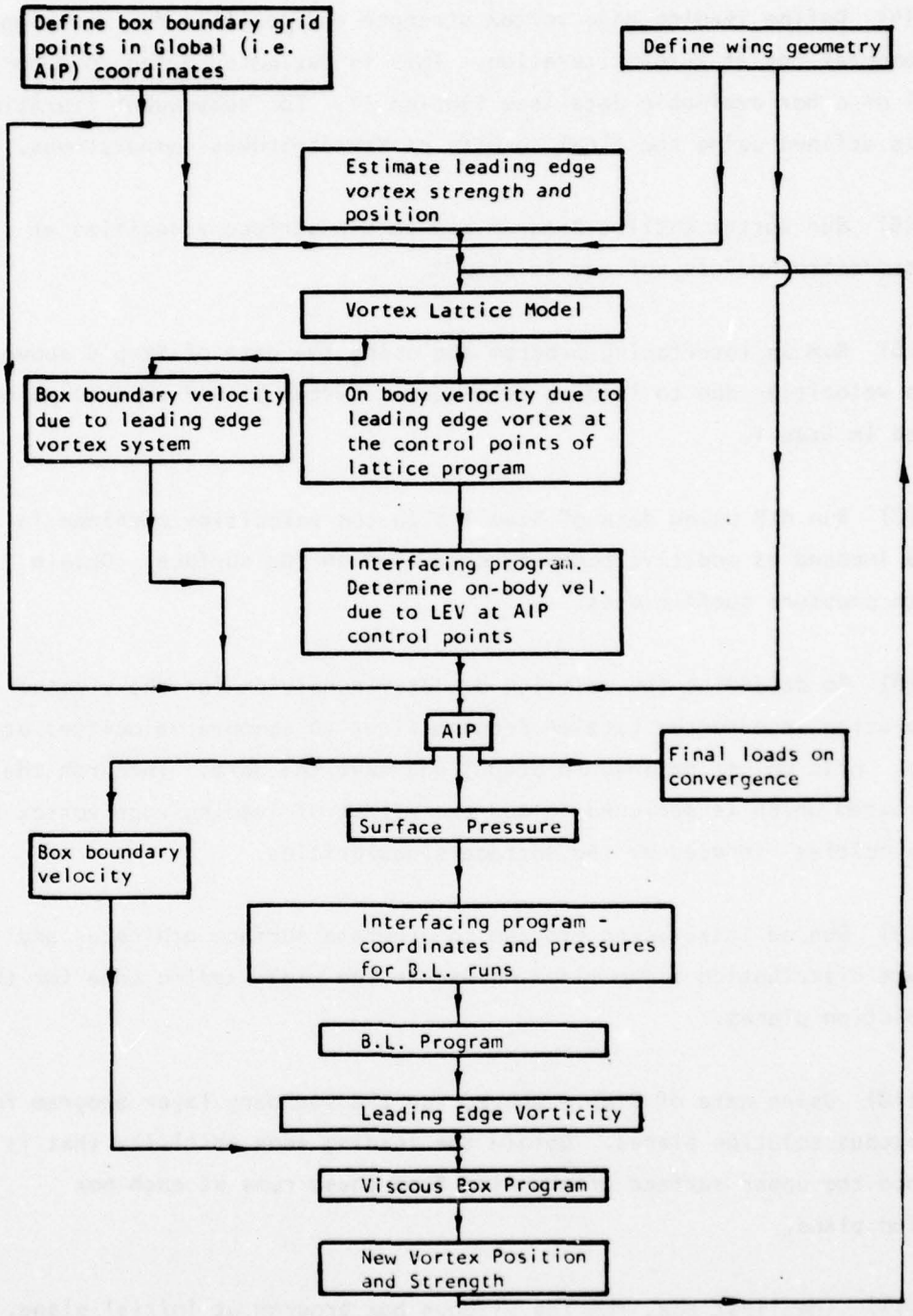

Figure 2.3. Computational Flow Chart

(4) Define leading edge vortex strength and position for starting the computations at zeroth iteration. This is estimated based on experimental or other available data (see Section 3). For subsequent iteration this is defined using the final results of Navier-Stokes computations.

(5) Run Vortex Lattice Program and obtain surface velocities at lattice control points defined in Step 2.

(6) Run an interfacing program and using the data of Step 5 above, obtain velocities due to leading edge vortex system at AIP control points defined in Step 1.

(7) Run AIP using data of Step 1 with the velocities obtained in Step 6 imposed as additive boundary condition on the surface. Obtain surface pressure coefficients.

(8) To determine the velocity boundary condition for the viscous box solution, run Vortex Lattice Program first to compute velocities at the box grid points defined in Step 3 and save the data. Then run the AIP program which is designed to add the effect of leading edge vortex to the velocities induced by the surface singularities.

(9) Run an interfacing program to generate surface ordinates and pressure distribution along lines normal to the wing leading edge for the box solution planes.

(10) Using data of Step 9 above, run the boundary layer program for the viscous solution planes. Obtain the leading edge vorticity that is fed onto the upper surface of the wing from these runs at each box solution plane.

(11) The first box, run the viscous box program at initial plane. Use very small ΔX values and large number of iterations, approximately 20, between velocity transport equation and Poisson's equation for velocity. Define the resultant solution as the initial conditions (see Section 5.2).

(12) With the initial conditions obtained above in Step 11, the velocity boundary conditions determined in Step 8, and the leading edge vorticity values of Step 10, run the viscous box program for all the boxes.

(13) From the vorticity distribution of viscous solution, define a new vortex position and strength. If the position and strength have not converged within acceptable limits, repeat calculations from Step 4. If they have converged, run the potential models alone once to obtain final pressure distribution on the surface and the force and moment coefficients.

3. POTENTIAL FLOW MODELS

The potential flow calculations are carried out using two separate programs. A vortex lattice program models the leading edge vortex system and computes the velocities induced by such a system at chosen points in the field. The velocities computed on the wing surface are imposed as additional boundary condition in a second program known as Aircraft Interference Program (AIP), which models the thick wing using singularity distributions on the wing surface.

3.1 Vortex Lattice Program

Figure 3.1 illustrates the free vortex system. For clarity only one vortex element is shown while the actual computations use 20 such vortex elements. The bound part of the vortex filament is located at the wing center plane and the free element is allowed to change direction when it meets the other filaments. To start with the vortex geometry and the circulation strengths are estimated from data available through experiments or any other empirical procedure. On subsequent cycles of iteration, the vortex system is reconstructed from the vorticity distributions obtained by the viscous box solution. Once the vortex geometry and the circulation strengths are completely specified, the vortex lattice program computes the velocity at any chosen point in the field using Bio-Savart's law.

The initial free vortex core position and strength has been estimated by the methods described in reference 11 with an additional modification to account for the effect of a rounded leading edge. The effect of the rounded leading edge is obtained from evaluation of experimental data comparing sharp and rounded leading edge in reference 12. Resulting equations for these vortex characteristics are:

$$\frac{Y_V}{C_R} = .32035 \frac{X}{C_R}$$

$$\frac{Z_V}{C_R} = \frac{Z_t}{C_R} + 0.05782 \frac{X}{C_R}$$

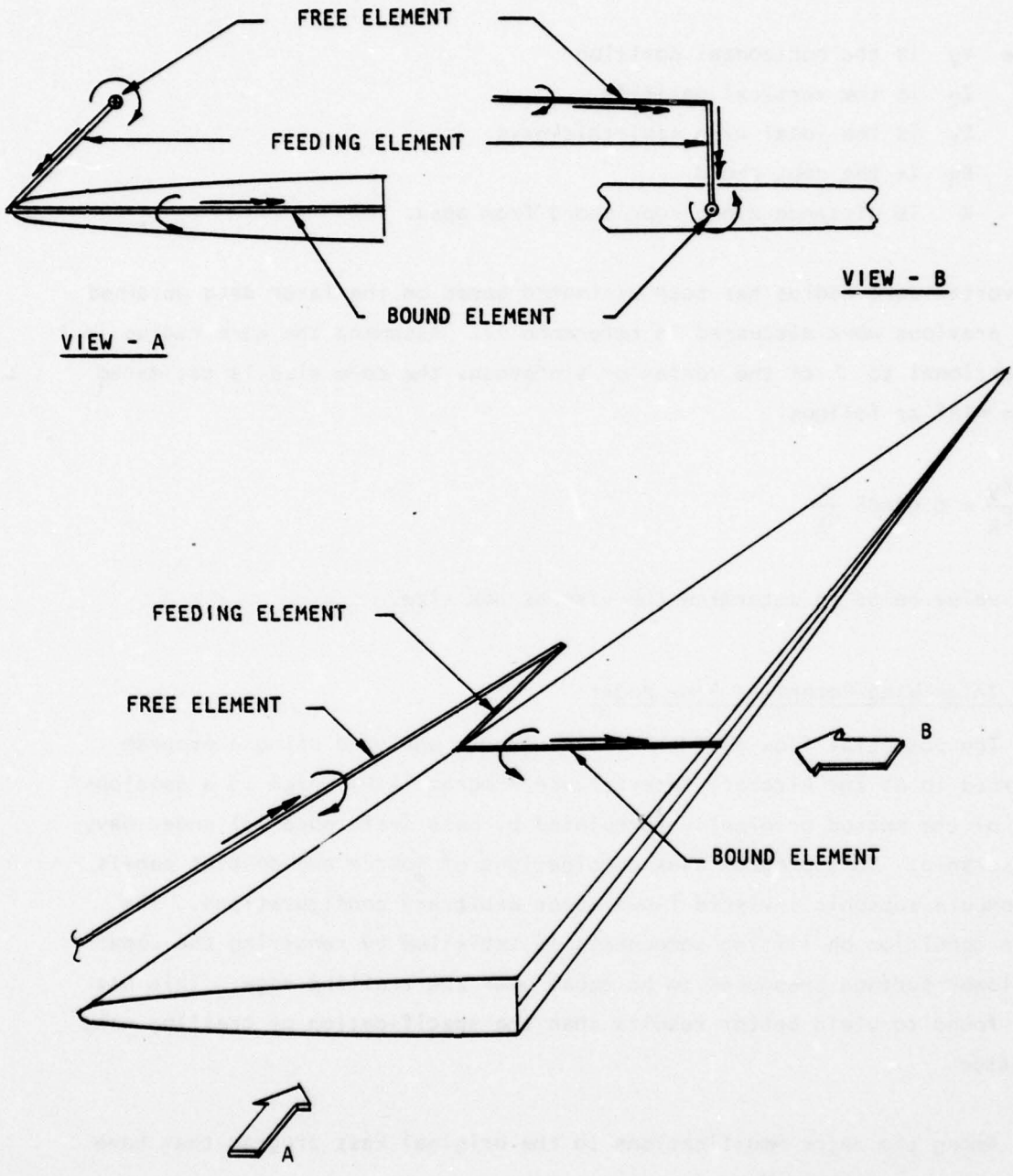

Figure 3.1 Free Vortex System Showing One Typical Element

$$\frac{2.35\Gamma}{U_\infty CR} = 0.5380\,\frac{X}{C_R} - 0.01281\,\left(\frac{X}{C_R}\right)^2 - 0.007226\,\left(\frac{X}{C_R}\right)^3 - 0.1248\,\left(\frac{X}{C_R}\right)^4$$

where Y_V is the horizontal position

Z_V is the vertical position

Z_t is the local wing semi-thickness

C_R is the root chord

X is distance along root chord from apex.

The vortex core radius has been estimated based on the laser data obtained from previous work discussed in reference 11. Assuming the core radius is proportional to Γ of the vortex or $\sin^2\alpha\cos\alpha$, the core size is estimated for $\alpha = 14°$ as follows.

$$\frac{R_V}{C_R} = 0.02008\,\frac{X}{C_R}$$

This value helps to determine the viscous box size.

3.2 Thick Wing Potential Flow Model

The potential flow past the thick wing is analyzed using a program referred to as the Aircraft Interference Program (AIP) which is a development of the method originally formulated by Hess (reference 13) under Navy sponsorship. This program uses combinations of source and doublet panels to compute subsonic inviscid flows about arbitrary configurations. The Kutta condition on lifting components is satisfied by requiring the upper and lower surface pressures to be equal near the trailing edge. This has been found to yield better results than the specification of trailing wake position.

Among the major modifications to the original Hess program that have been made at Lockheed-Georgia are:

(1) Improved coding to eliminate errors in the originally acquired program and to make the program computationally more efficient.

(2) Modified program input and output making it easier to use.

(3) Development of a configuration loft program to automatically determine component intersections and to permit visual verification of the paneling.

The AIP program has the capability of providing surface velocity components and pressures, aerodynamic forces and moments, and off-body flow field information. The program is currently applicable to arbitrary configurations for which viscous effects can be neglected. Figures 3.2 and 3.3 show a typical transport configuration and attendant wing surface pressures. The lack of agreement between theory and experiment evident in the lower surface pressure comparisons occurs because the pylons and nacelles were not included in the theoretical calculations. The slight over-prediction of upper surface pressures is attributable to the neglect of viscous effects. The good agreement between theory and experiment evident in the vicinity of the leading edge is of particular significance for the subject study. These calculations were performed with 528 surface panels and require approximately 161 seconds computation time on a CDC 7600 computer. Less computer time is required for lower Mach numbers.

3.3 Integration of Vortex Lattice Model and AIP Program

The effect of the leading edge vortex system on the wing is established by the inclusion of its induced velocities, as determined by the Lattice Program, in the boundary conditions at the AIP program's collocation points on the wing. The computed results of AIP program will then reflect the presence of the leading edge vortex. Also, at the boundary grid points of viscous box program, the velocities are determined by adding the velocities at these points obtained through AIP program as stated above to the velocities induced by the leading edge vortex system itself.

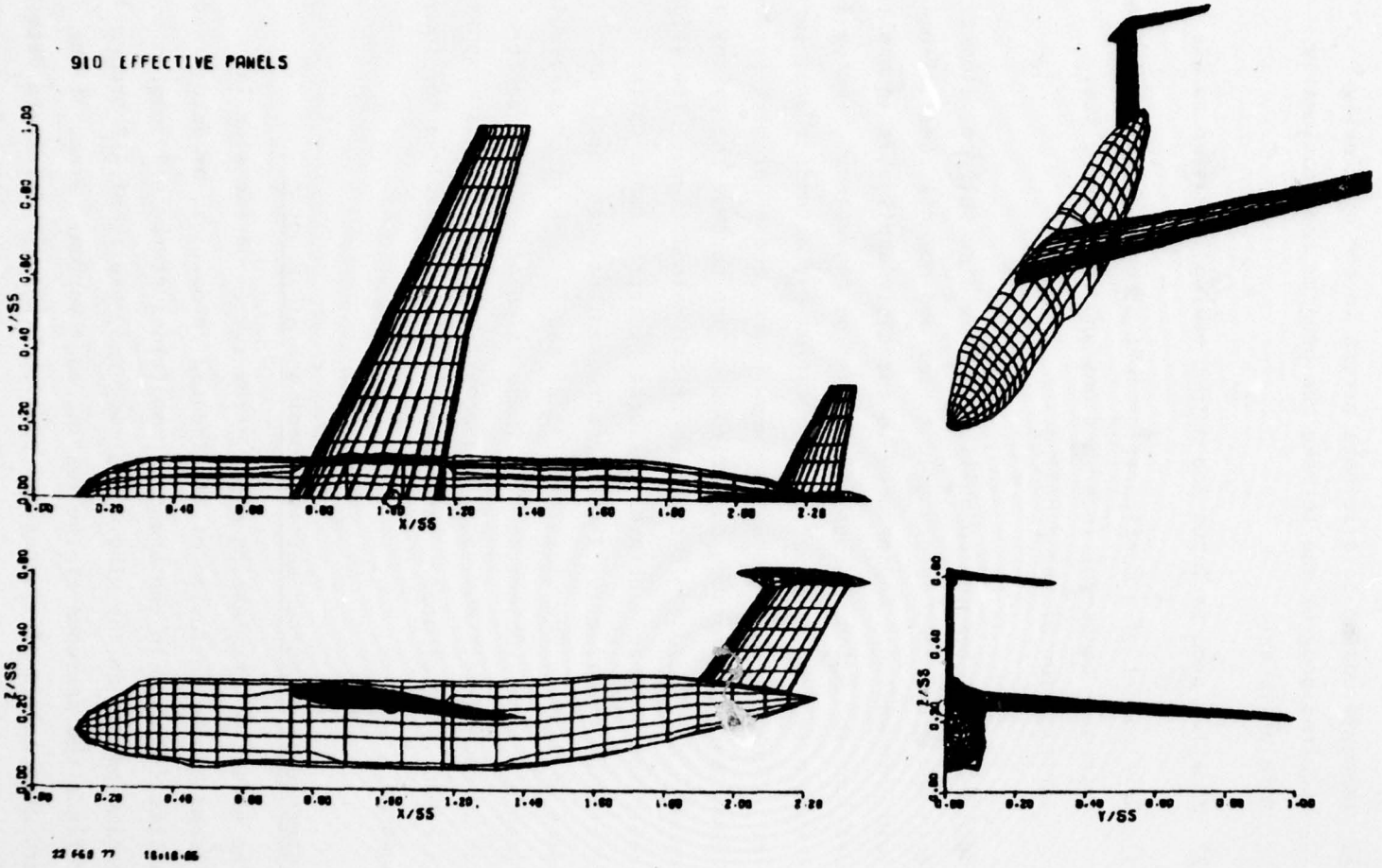

Figure 3.2 Panels for C-5A Wing/Fuselage/Empennage

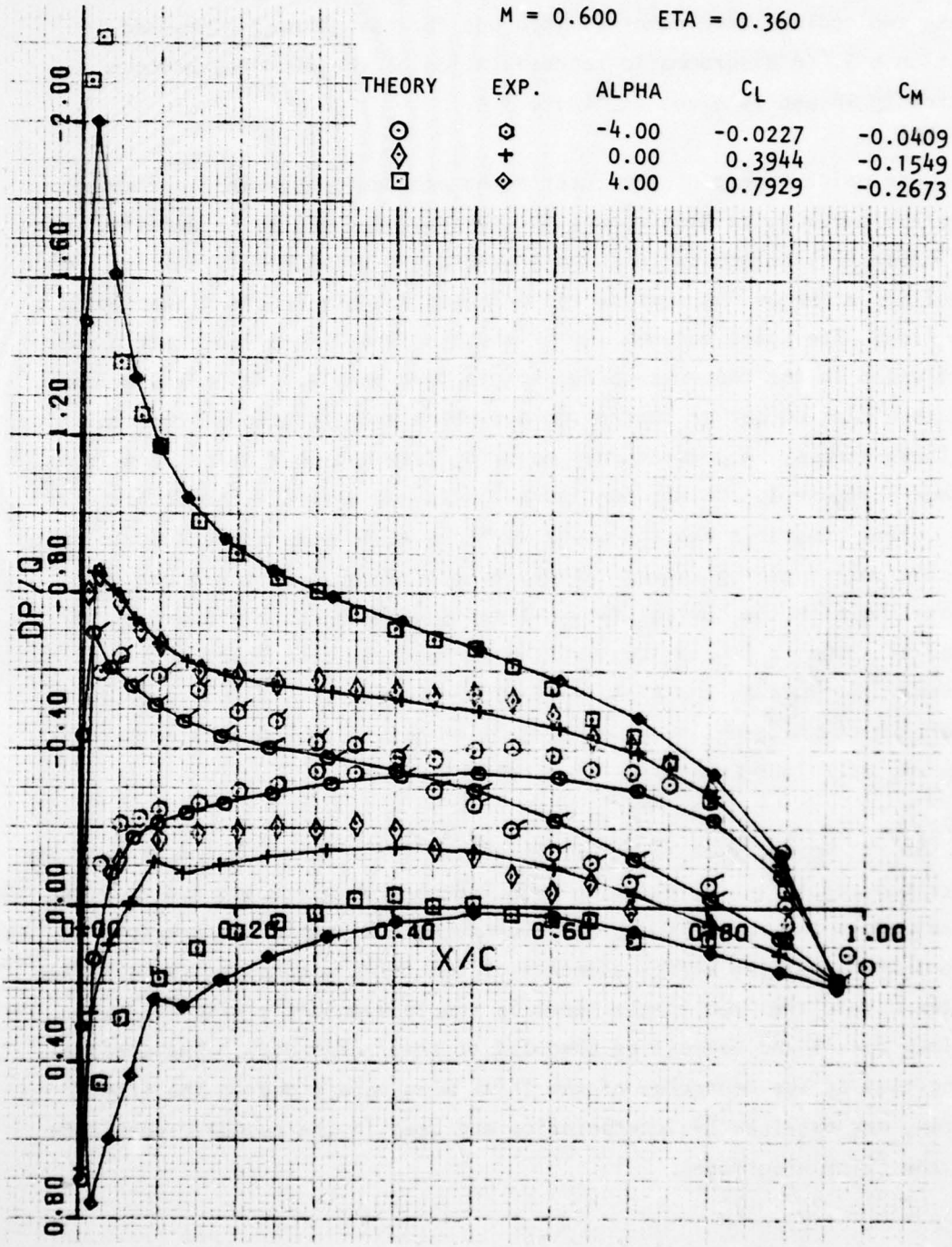

Figue 3.3 Pressure Distributions for C-5A Wing at 36.9% Span

Initially the two potential flow programs were organized to run separately with an additional peripheral program to integrate the results. This was considered a desirable feature during the development stage, but these two codings were combined into one for case 4 runs discussed in Section 6.3. A diagrammatic representation of the coupling process currently in use is given in figure 3.4.

One major aspect of the interfacing procedure between these two programs needs to be mentioned. The conventional method of paneling wings and other lifting bodies in the AIP program is by means of "n lines" which are lines drawn on the surface and oriented roughly in the direction of the flow. The space between two of these n lines is called a strip which is divided in the chordwise direction to form panels. All calculations are then carried out at control points which are situated at the centroids of these panels. A conventional paneling laid out on a delta wing is as shown in figure 3.5. This configuration is not entirely compatible with the vortex program since the bound vortices would pass very close to the control points giving uneven velocity distribution. On the other hand, a paneling with the conical flow n-lines converging to the apex of the wing, as shown in figure 3.6, for the AIP program, was found to give uneven variations of the field variables. Further, it also proved very sensitive to the paneling; i.e. a small change in the panel sizes at the apex caused a 100% change in lift coefficient.

So, it was decided to revert to conventional panelling and after some experimentation, a configuration with 218 panels was chosen and provided satisfactory accuracy without undue computational time. To prevent interference between vortex elements of the thick wing model and the free vortex model, the free vortex model is run independently with its own optimum panels and velocities computed at their centroids. The surface velocities at the centroids of the thick wing panels due to the free vortex, are obtained by interpolation and used in the boundary condition for the thick wing model.

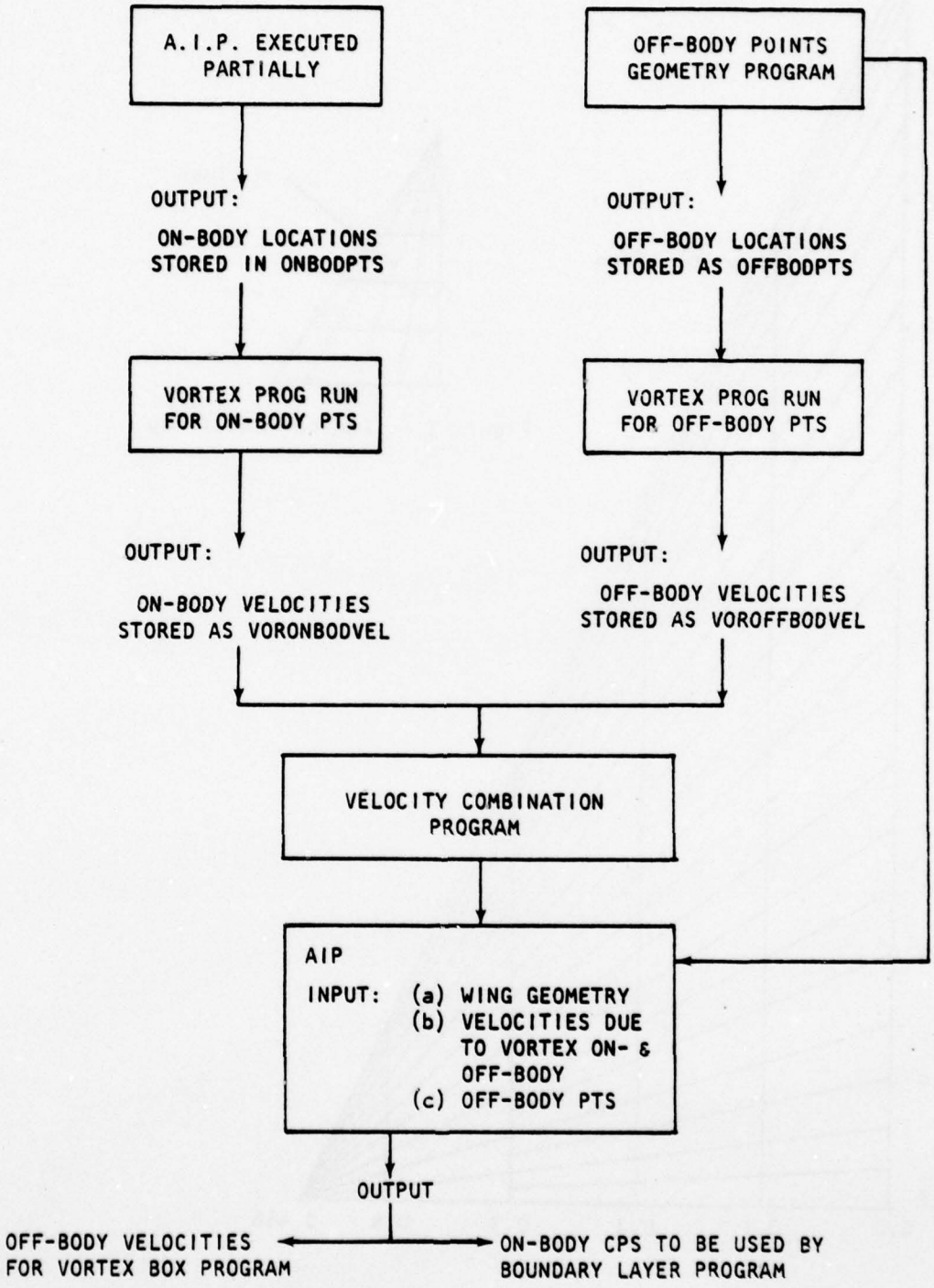

Figure 3.4 Potential Flow Integration Program

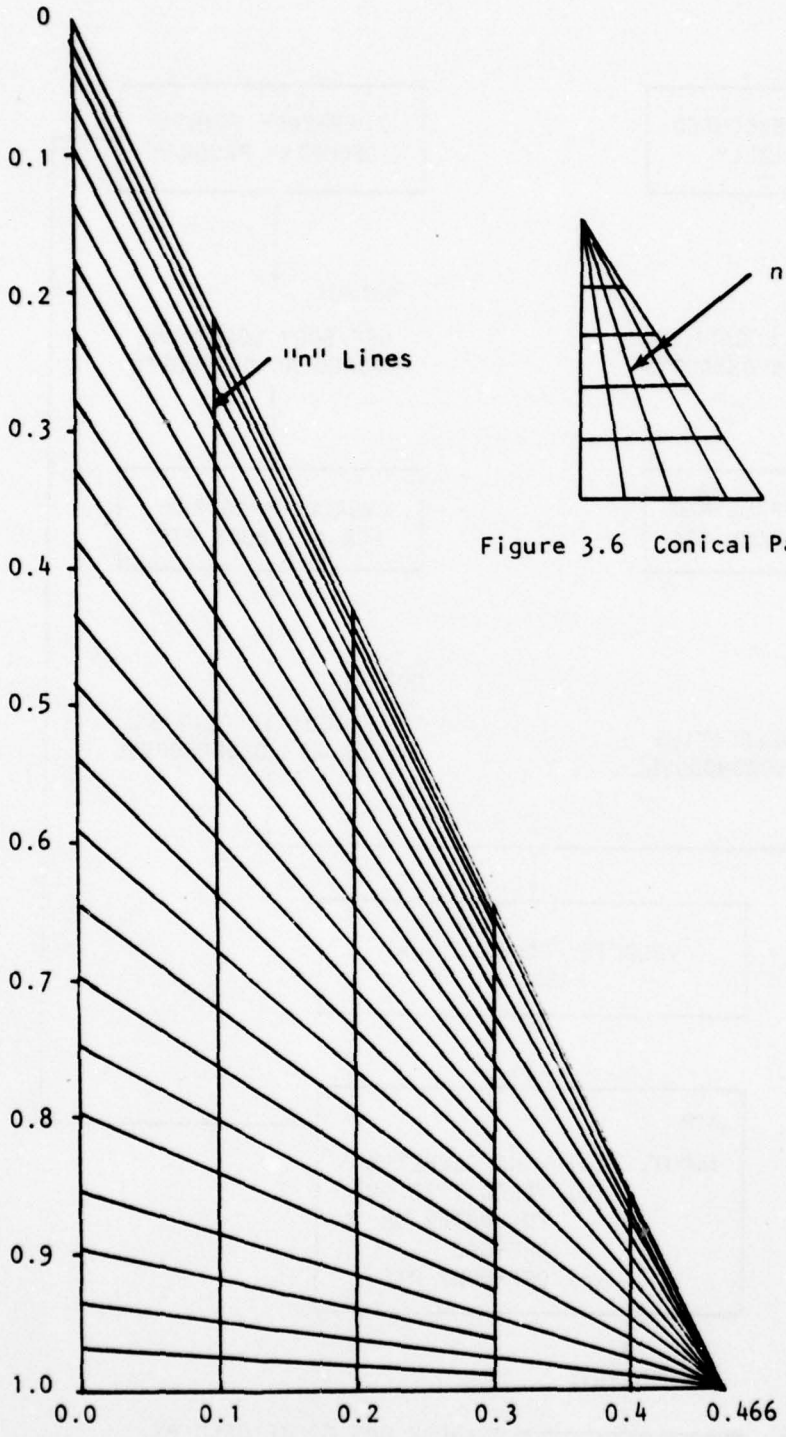

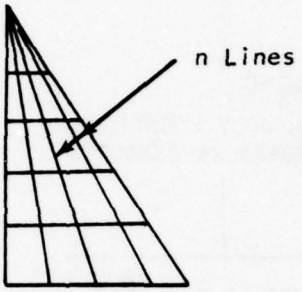

Figure 3.6 Conical Panelling

Figure 3.5 Conventional Panelling

4.0 BOUNDARY LAYER PROGRAM

4.1 Requirement for Leading Edge Vorticity

As indicated in reference 11 and in Sections 1.0 and 2.0, it is imperative to know the strength and spatial orientation of the vorticity shed at the leading edge. This parameter is a function of local angle of attack, circulation and the shape of the leading edge. These conditions in turn determine the local pressure distribution and the boundary layer characteristics. Since the configurations of concern are usually swept and three-dimensional, a 3-D boundary layer program that can predict the boundary layer characteristics very near flow separation is required. In some cases vortex shedding (flow separation) does not occur until slightly aft of the leading edge (for airfoils having leading edge separation as opposed to trailing edge separation). For these cases it is useful and more accurate to have the boundary layer as thick as possible in order to cross a multiple number of viscous box mesh points as the boundary layer enters the box. Strictly speaking, it is required to compute a boundary "region", i.e. a region including higher-order effects than those occurring in first-order boundary layer theory (see figure 4.1). In order to establish with accuracy the forward edge velocity and vorticity values for the box, it is necessary to perform a computation from the wing attachment line through the boundary layer and into the second order, rapidly thickening, boundary layer region. This technique not only provides a thick boundary layer but it brings the boundary layer solution very close to separation. It is assumed, therefore, when the forward marching, parabolic boundary layer solution "blows-up" the boundary layer separates. This allows one to determine at high Reynolds number if there is in fact leading edge separation. Recognizing the sensitivity of the viscous box vortex flow region to the vorticity imposed by the leading edge boundary layer region, it is essential that three dimensionality be accounted for in any model of the boundary region. For this purpose, it is deemed necessary and sufficient to apply the "infinite yawed wing" assumption. This method has proven quite effective in the analysis of boundary layers near attachment lines and even for some complete wings of sufficiently high aspect ratio, as shown by Nash and Tseng[14]. Using the three-dimensional boundary layer methods of Nash and Patel[15], Nash and

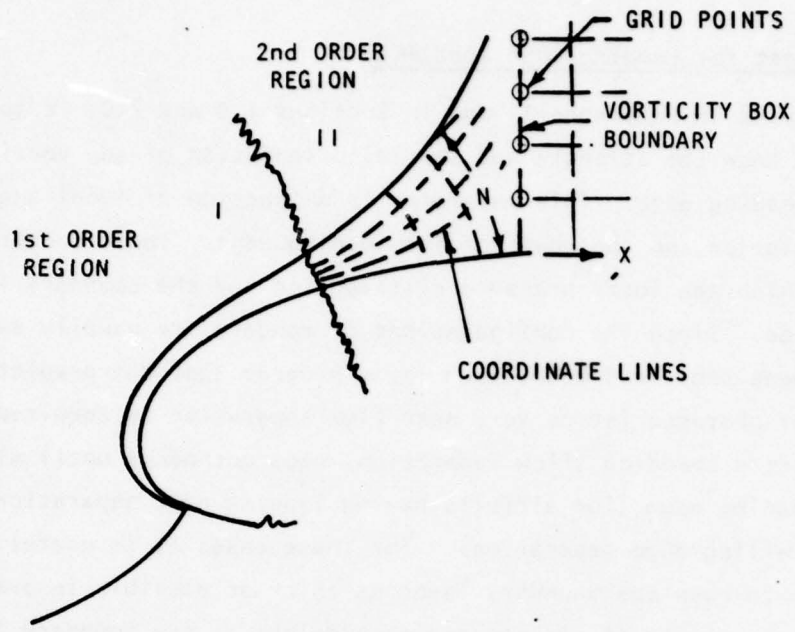

Figure 4.1 Section Showing Boundary Layer First and Second Order Domains

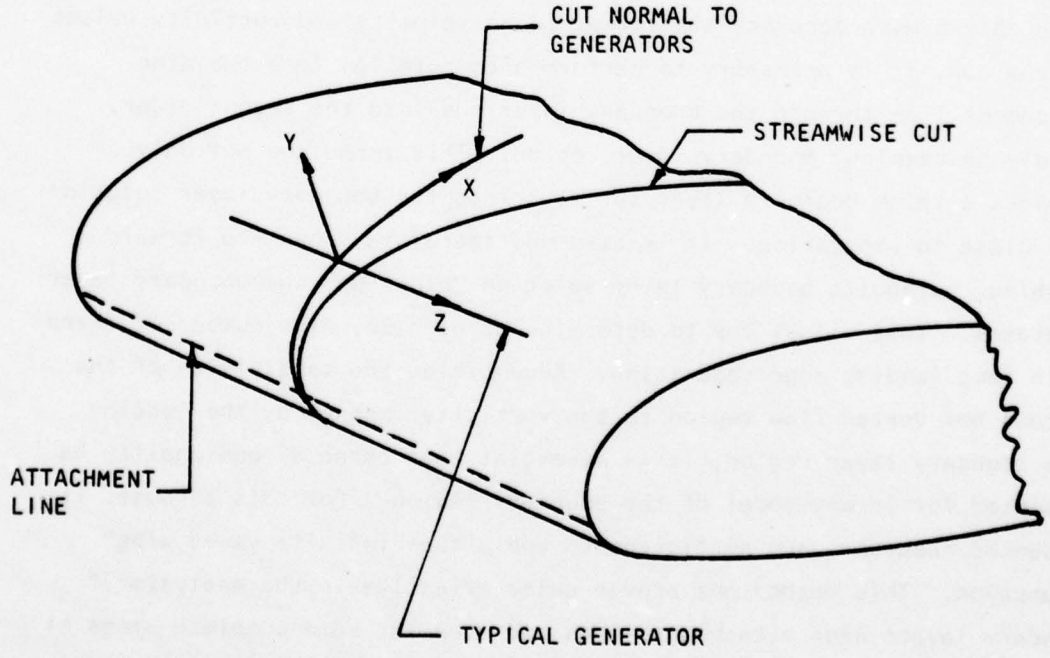

Figure 4.2 Wing Section Showing Boundary Region Coordinate System

Scruggs as consultants to Lockheed developed the infinite yawed wing, second-order boundary layer program for the current effort.

4.2 Second-Order Boundary Layer Method

In order to approximate the flow upstream of the viscous box boundary, the usual boundary layer assumptions must be augmented by the appropriate second-order effects. Since the boundary region experiences rapid increase in thickness and considerable turning of the flow in the spanwise direction, two additional effects must be represented: three-dimensionality and normal pressure gradient. For the first of these requirements it was deemed adequate to assume, at least locally, that the flow is of the infinite yawed cylinder type. This retains three-dimensionality but permits much faster computation of the flow field. In this case the metric on the wing surface is

$$ds^2 = (h_1 dx)^2 + (h_2 dy)^2 + dz^2 \tag{4.1}$$

where, as shown in figure 4.2 the coordinate x is measured along lines normal to the wing leading edge and z is measured along the generators. The first-order boundary layer momentum equations are then

$$\frac{U}{h_1}\frac{\partial U}{\partial x} + \frac{V}{h_2}\frac{\partial U}{\partial y} + \frac{1}{h_1}\frac{\partial}{\partial x}\left(\frac{p}{\rho}\right) + \frac{1}{h_2}\frac{\partial \overline{uv}}{\partial y} - \frac{\nu}{h_2^2}\frac{\partial^2 U}{\partial y^2} = 0 \tag{4.2}$$

$$\frac{U}{h_1}\frac{\partial w}{\partial x} + \frac{V}{h_2}\frac{\partial w}{\partial y} + \frac{1}{h_2}\frac{\partial \overline{wv}}{\partial y} - \frac{\nu}{h_2^2}\frac{\partial^2 w}{\partial y} = 0 \tag{4.3}$$

The turbulent kinetic energy equation is also solved to obtain the turbulent shear stresses. The well-documented method of Nash[15] is used to model the shear stresses in terms of turbulent kinetic energy. The continuity equation is used to solve for normal velocity, V.

In order to allow for normal pressure gradients in the case of a rapidly thickening domain, a second order approximation is required. This takes the form of an approximation to the normal momentum equation:

$$K_{21}UV - K_{12}U^2 + \frac{1}{h_2}\frac{\partial}{\partial y}\left(\frac{p}{\rho}\right) = 0, \qquad (4.4)$$

where K_{21} and K_{12} are curvatures of the coordinate system. The numerical method utilizes a curvilinear coordinate system, which is evolved as the flow develops in the downstream direction. Thus (see figure 4.1) the two curvatures can be computed at each step of the solution in the stream direction. The continuity equation in this system takes the form,

$$\frac{1}{h_1}\frac{\partial U}{\partial x} + \frac{1}{h_2}\frac{\partial V}{\partial y} + K_{21}U = 0. \qquad (4.5)$$

The procedure used to solve the second order approximation involves a retrospective treatment of equation (4.4). The basic scheme used for the first-order boundary layer solution is well tested and in this manner the essential features of that scheme can be retained. The schematic in figure 4.3 summarizes the iterative procedure used to compute the higher order flow. Pressures provided by the potential flow solution are applied at the wing surface. Following a first solution of the boundary layer equations, an incremental pressure gradient is found retrospectively from the normal momentum equation such that the flow curvatures are balanced. The incremental pressure variation through the layer is found by integrating the normal momentum equation from the wall to the outer edge of the layer. This increment is then differentiated with respect to x and added to the previous pressure gradient used in the boundary layer equations. Thus, $\partial p/\partial x$ appearing in equation (4.2) becomes a function of both x and y. The new $\partial p/\partial x$ implied at the edge of the layer is used in the Euler equations to obtain new edge values of velocity. The calculation then returns to the boundary layer equations for a new iteration and the procedure is continued to convergence.

The basic numerical procedure is similar to that used in the vorticity box method (Section 5) but with some modifications to treat the present problem. The scheme is forward marching and as such requires initial conditions. These initial conditions at the attachment line depend on the value of wing sweep. Beyond about 25° the flow is turbulent. For the case of a laminar leading edge, exact attachment line solutions are available

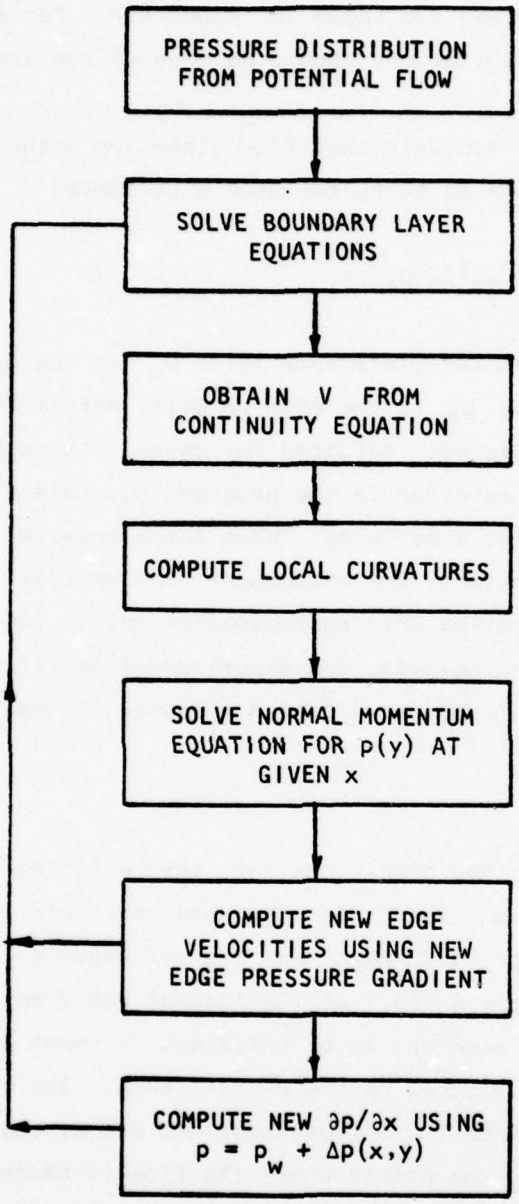

Figure 4.3 Boundary Layer Iterative Procedure

to start the computation. These solutions for U and W as a function of y, and near the attachment line, are shown in figure 4.4. For a turbulent leading edge appropriate modifications should be made to the profiles.

It has been shown experimentally that flow along the attachment line of an infinite swept wing will be turbulent when a parameter

$$C^* = w_e^2/\nu\partial U_e/\partial x,$$

exceeds a value of about 1.4×10^5 (reference 16). W_e is the edge velocity along the attachment line and U_e is the edge velocity normal to the attachment line. Turbulent flow was not indicated for cases 1 through 3 of these investigations due to an error in the program, but case 4 does predict turbulent flow as expected for a 65° wing. When turbulence is indicated, it is current practice to approximate the attachment line profile via a power law. For the present application this approximation may be too crude. If computational experiments so indicate, the experimental profiles of Cumpsty and Head (reference 16) should be curve fitted and used instead.

4.3 Boundary Layer Results

Calculations by this method have, thus far, been well-behaved; the number of iterations required has not increased and no stability problems have been encountered. Figure 4.5 shows some typical results from the boundary layer program for the airfoil at the face of box 2 on the 65° delta wing. The calculated boundary layer thickness is shown as a function of the airfoil chord and as plotted on the airfoil nose. The pressure gradient is highly adverse from the airfoil nose and aft as the plot of C_p shows. Also illustrated are the points where the flow is caused to be turbulent and where the normal momentum equation is put into action (dC_p/dN 0). Between X/C = .0012 and .0016 the flow separates since the boundary layer program "breaks down" at X/C = .0016. A finer X/C choice aft of X/C = .0012 would have been desirable to obtain the separation point more accurately, and therefore be a little more accurate on the rate of vorticity shed from the boundary layer. Figure 4.6 shows the boundary layer profile at X/C = .0012, just prior to separation. The inflection in the profile indicates an approach to separation.

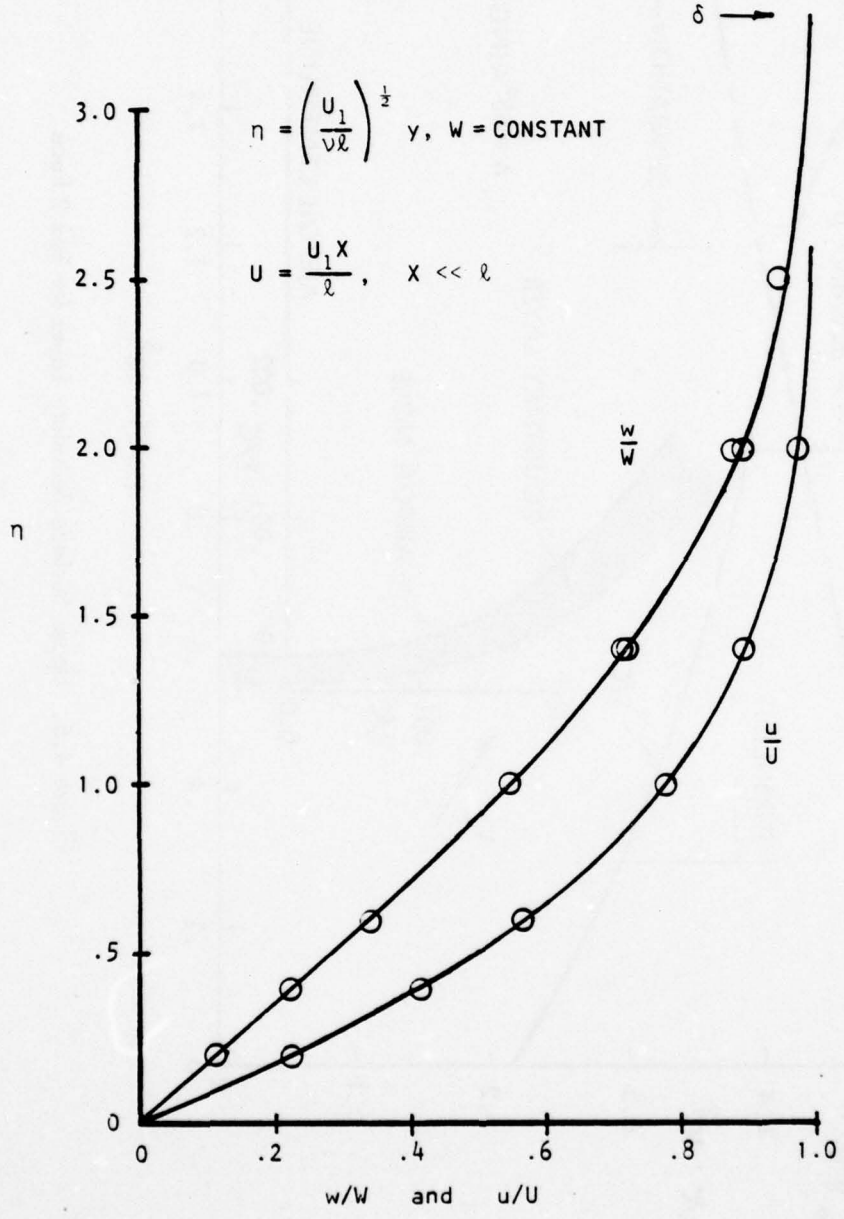

Figure 4.4 Stagnation Line Flow — Infinite Yawed Cylinder

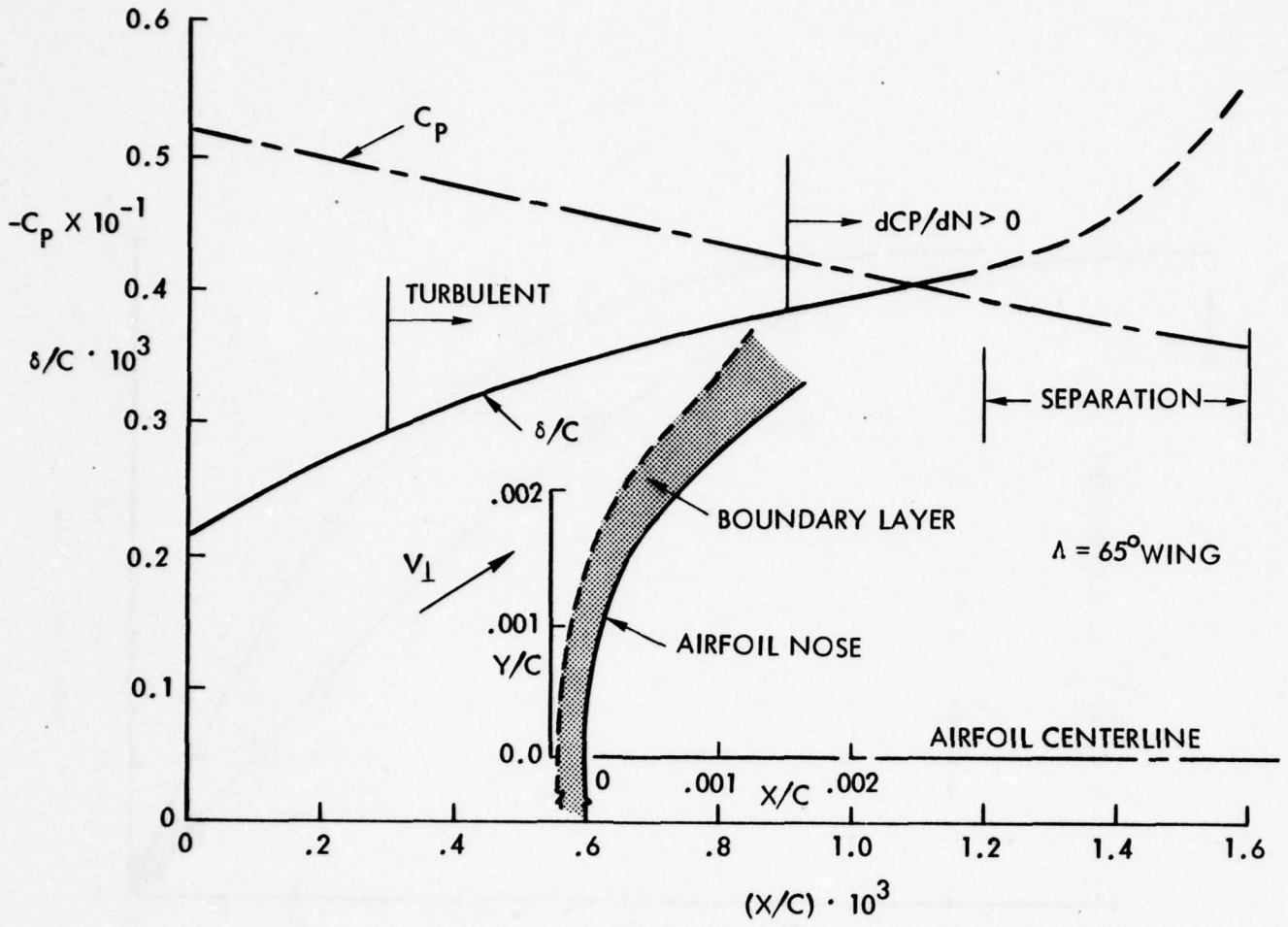

Figure 4.5. Upper Surface Boundary Layer for Box 2 Face

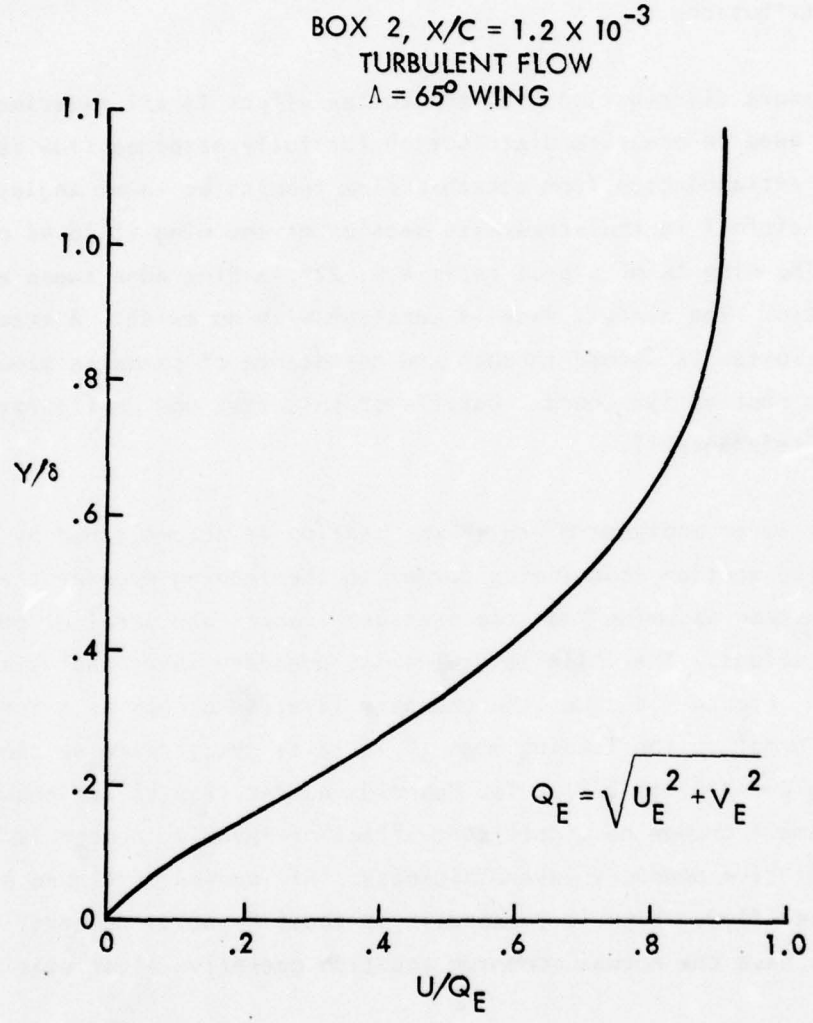

Figure 4.6. Boundary Layer Profile Near Flow Separation

More detailed investigations of the boundary layer program results were made on another wing for which experimental pressure data are available and a leading edge vortex is formed. This wing has a very blunt leading edge but there is leading edge separation making it ideal to test the boundary layer program. Figure 4.7 shows the airfoil and experimental pressure distributions.

The pressure distribution with the vortex effect is all experimental; however, the adverse pressure distribution for fully attached flow is estimated by extrapolation from attached flow results at lower angles of attack. The airfoil is the streamwise section of the wing at 36.4% of the wing span. The wing is of aspect ratio 4.0, 22° leading edge sweep and 0.7 taper ratio. The airfoil type is constant with no twist. A steady leading edge vortex is formed through the assistance of spanwise blowing from the wing root at 33% chord. Details of this test and configuration are given in reference 17.

Boundary layer analyses of this wing section is accomplished by first determining the section coordinates normal to the leading edge at the 36.4% span position then assuming that the pressure isobars are parallel to the constant X/C values. The infinite yawed wing boundary layer analysis is then applied. Figure 4.8 shows the boundary layer thickness as a function of the X_N/C normal to the leading edge (C is still the streamwise chord; therefore, $X_N/C = (X/C)\cos 22°$). Two Reynolds number results are shown, and for the small change no significant effect of Reynolds number is found except the relative boundary layer thickness. All curves of figure 4.8 are for laminar flow, which is reasonable at these Reynolds numbers. Two of the curves have the normal momentum equation operative after station 9 ($X_N/C = .023$).

The low Reynolds number of figure 4.8 is the actual experimental value based on the streamwise chord length of 8.2834 cm (0.44 ft). For this case, boundary layer stations have been analyzed to come close to the separation point. Initially, no data were obtained between stations 9 and 11 and this produced a slightly different curve (not shown). Also, well beyond station 13 convergence could not be met; therefore, closer

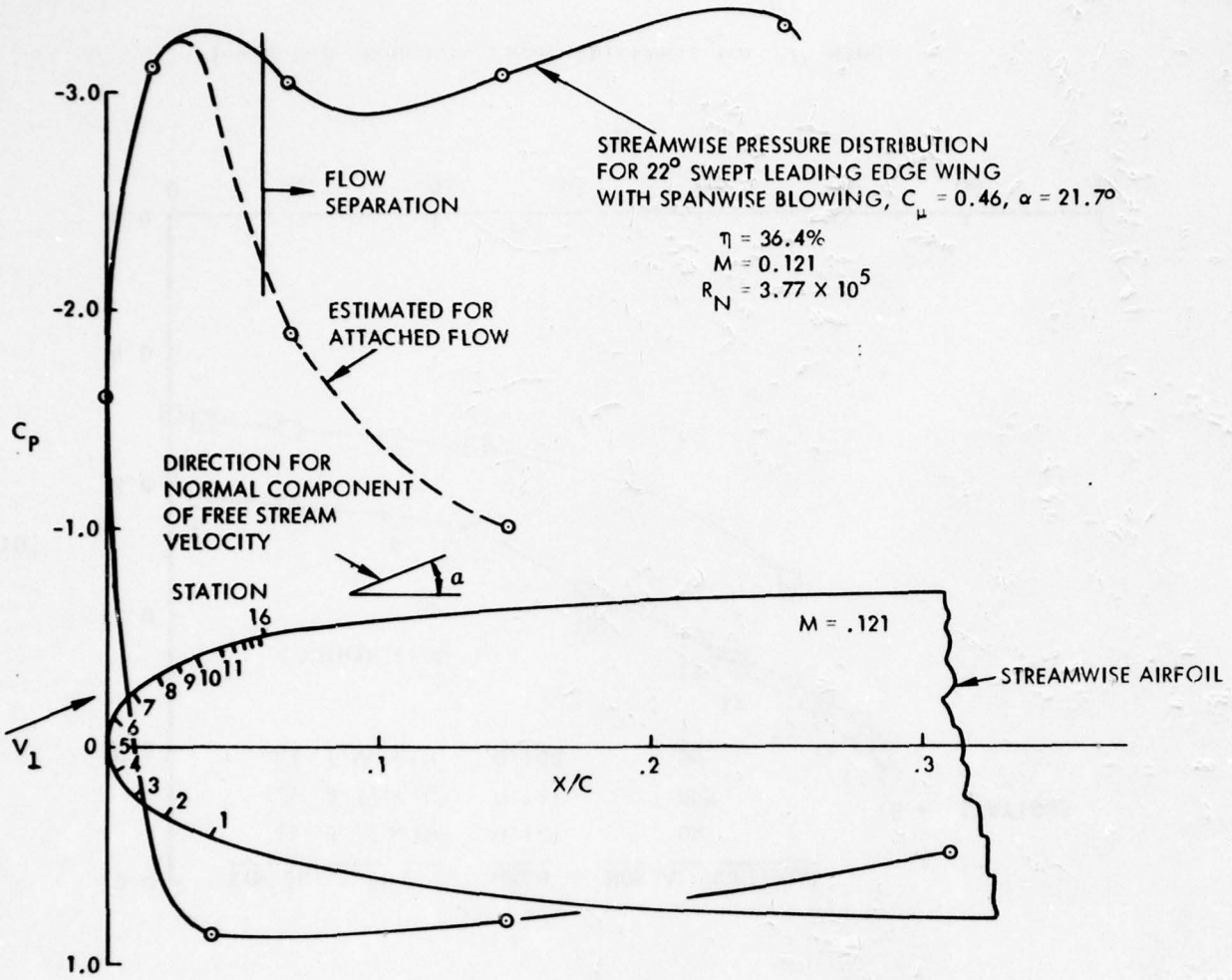

Figure 4.7 Boundary Layer Program Test Model, $\Lambda = 22^\circ$

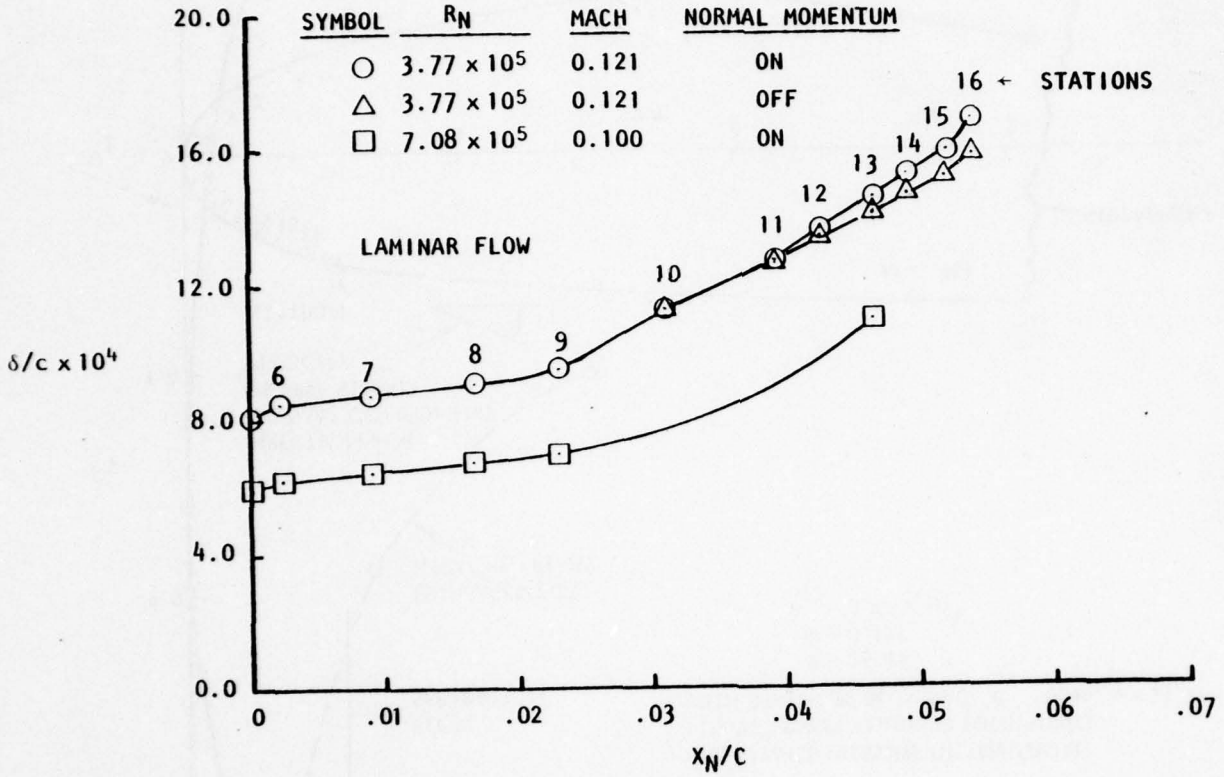

Figure 4.8 Boundary Layer Thickness for 22° Wing

data points around station 13 were input to the program. In the second trial, with station 10, included along with points beyond 13, separation is not indicated until just slightly past $X_N/C = .054$. It is interesting to note that in this case figure 4.8 shows that without the normal momentum equation operating separation occurs at about the same place. The boundary layer thickness is somewhat smaller though.

Figure 4.9 shows the boundary layer profiles for stations 9, 14, 15, and 16 for the lower Reynolds number data. The progression towards a separated profile is obvious with that at station 16 coming very close to the separation point. Ideally the program should be run at more points until the initial separation profile is found, i.e. with $\partial u/\partial y = 0$ at the surface.

The separation point is approximated at $X_N/C = .054$ or $X/C = .058$. As shown on figure 4.7, this is in good agreement with the separation indicated by the experimental pressure distribution. It is important to note that, if the actual experimental pressure distribution is used with its relatively low adverse pressure gradient, no separation occurs in the boundary layer program. It was therefore necessary to estimate the distribution as shown in figure 4.7 for attached flow. After some thought, this is considered the most accurate technique. The boundary layer program is designed for attached flow only, even though the second-order modification brings it close to separation; therefore, the correct technique is exactly what is done in the theoretical approaches of the following sections. The attached flow pressure distribution at the appropriate angle of attack and in the presence of the leading edge vortex is input to the boundary layer program. No leading edge vortex sheet is included for this would change the flow field that should be analyzed by the boundary layer program. *Note: Results from Case 4 in Section 6.3 suggest that the influence of the free vortex should also be eliminated because leading edge pressures are not correct until vortex converges to correct position.* Once the separation point is established though, the vortex sheet and the secondary vortex would improve the potential flow pressure distribution.

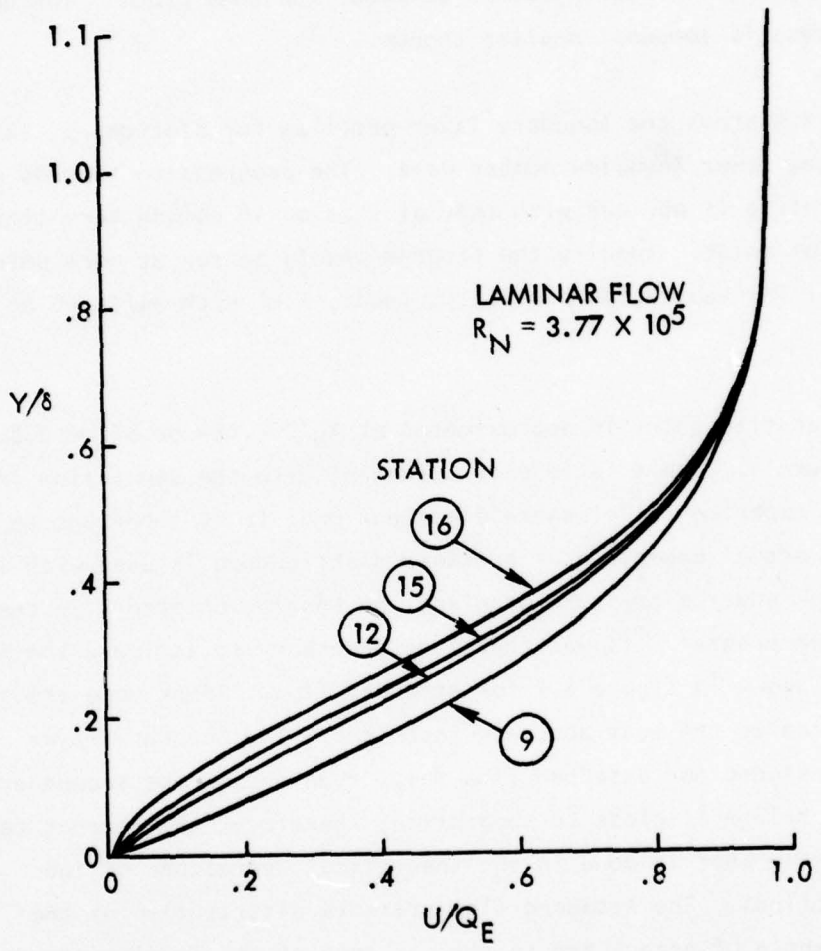

Figure 4.9. Boundary Layer Profiles Near Separation, $\Lambda = 22^\circ$ Wing

It is also important to note that separation did not occur when turbulence was initiated at station 7 for the 7.08×10^5 Reynolds number. (*Note: Transition is artificial and this R_N would probably not cause turbulence.*) The flow was attached all the way to X/C = .15 even using the attached flow pressure distribution. The significance of this is that at high Reynolds numbers where transition occurs naturally there will be no leading edge separation and therefore no leading edge vortex. This may be a real problem for configurations like the space shuttle and future supersonic transports that are designed to take advantage of the leading edge vortex. Even on fighter aircraft where the wings are thin, this phenomenon will determine at what angle the vortex forms and at what position (affecting the moments and stability). *It is very important that a high Reynolds number boundary layer program be used to determine where, how, and how much vorticity (circulation) is fed to the leading edge vortex.* (See Case 4, Section 6.3.)

4.4 Application of Boundary Layer Program

As noted previously, the output required from the boundary layer is the vorticity, its strength, and direction. More specifically, the rate of circulation shed from the boundary layer in all three directions is the required output from the boundary layer program.

The total rate of circulation for each component of vorticity using boundary layer coordinates transferred to box coordinates is given below. (Figure 4.1 illustrates how the boundary layer thickness occurs along the curved coordinate.) For most practical purposes, however, δ can be assumed normal to the surface making

$$dz = dN \sin(\theta - \varepsilon) \quad \text{and} \quad dy = dN \cos(\theta - \varepsilon),$$

where θ is the airfoil surface slope.)

$$\frac{d\bar{\Gamma}}{dt} = \left[\int_0^{\delta\cos(\theta-\varepsilon)} \xi\, w\,dy + \int_0^{\delta\sin(\theta-\varepsilon)} \xi\, v\,dz \right]_{yz} \bar{i} + \left[\int_0^{\delta\sin(\theta-\varepsilon)} \eta\cos(\theta-\varepsilon)\, u\,dz \right.$$

$$\left. + \int_0^{\delta} \eta w\,dx \right]_{xz} \bar{j} - \left[\int_0^{\delta} \zeta\sin(\theta-\varepsilon)\, v\,dx + \int_0^{\delta\cos\theta} \zeta\cos(\theta-\varepsilon)\, u\,dy \right]_{xy} \bar{k} \qquad (4.6)$$

(The subscripts on the brackets indicate the plane to which the vorticity is normal.) For an infinite yawed wing dx is zero over the boundary layer height leaving only one term in each of the last two brackets.

If the direction of the velocity is not of concern

$$\frac{d\bar{\Gamma}}{dt} = \bar{i} \int_0^{\delta} \xi \sqrt{w^2+v^2}\, ds + \bar{j} \int_0^{\delta\sin(\theta-\varepsilon)} \eta\cos(\theta-\varepsilon) + \bar{k} \int_0^{\delta\cos(\theta-\varepsilon)} \zeta\cos(\theta-\varepsilon) \qquad (4.7)$$

The circulation per unit length, $\bar{\Gamma}/L$, can be written as

$$\frac{\bar{\Gamma}}{L} = \frac{\bar{i}}{\sqrt{\bar{w}^2+\bar{v}^2}} \int_0^{\delta} \xi \sqrt{w^2+v^2}\, ds + \frac{\bar{j}}{u} \int_0^{\delta\cos(\theta-\varepsilon)} \eta u\,dy + \frac{\bar{k}}{u} \int_0^{\delta\sin(\theta-\varepsilon)} \zeta u\,dy \qquad (4.8)$$

However, the product of $\bar{\Gamma}/L$ and the average velocity in the boundary layer must remain constant for each component when transferring the circulation to the viscous vorticity box. That is, where the exact position of the boundary layer cannot be maintained because of the large grid size in the box, the value of $d\bar{\Gamma}/dt$ from equation (4.7) must be maintained. Therefore, the velocity at the nearest grid point will have to be changed to the average boundary layer velocity and equation (4.8) used for $\bar{\Gamma}/L$. Vorticity

per unit length is obtained by dividing the resulting $\bar{\Gamma}/L$ by the mesh length, Δy, of the box. This technique eliminates the confusion in transferring vorticity from the boundary layer to the box. Section 5 discusses this technique further, showing the relation between boundary layer dimensions and box dimensions.

Originally it was hoped that the grid points of the box would actually fall in the boundary layer as shown in figure 4.1. This was not practical for the current work for the number of mesh points in the box would be too large for practical computer time. A grid transformation technique would allow closer grid points near the boundary layer while stretching their distance apart further away from the boundary layer. Even when this occurs though it will be necessary to apply the constant rate of circulation concept at each grid point which must contain all the circulation over a finite distance of the boundary layer.

5. VISCOUS BOX CALCULATIONS

5.1 Governing Equations

With the boundary conditions provided by the potential flow and boundary layer calculations, detailed flow features are computed over finite integration domains by solving the Navier-Stokes equations. The governing equation is formulated as the vorticity transport equation,

$$\vec{V} \cdot (\vec{\nabla}\vec{\omega}) = \vec{\omega} \cdot (\vec{\nabla}\vec{V}) + \nu\nabla^2\vec{\omega} \tag{5.1}$$

where velocity and the derived variable vorticity given by

$$\vec{\omega} \equiv \vec{\nabla} \times \vec{V} \tag{5.2}$$

are used as the primary dependent variables. The velocities are computed by numerically solving the equation

$$\nabla^2\vec{V} = -\vec{\nabla} \times \vec{\omega}. \tag{5.3}$$

If the physical flow phenomena permits the assumption that diffusion is negligible in one of the coordinate directions (say x-direction) compared to the other two directions, then one can approximate the diffusion term as

$$\nabla^2\vec{\omega} = \left(\frac{\partial^2}{\partial y^2} + \frac{\partial^2}{\partial z^2}\right)\vec{\omega}.$$

This renders the partial differential equations, (5.1), to be parabolic thus enabling the usage of forward marching techniques. The integration domain for these governing equations are the so-called "Viscous Boxes", the orientations of which are shown in Figure 2.1. The details of the numerical procedure for solving these governing equations may be found in the earlier reports (refs. 9, 10, and 11). In the following sections refinements and further modifications introduced in the solution procedure are discussed.

5.2 Initial and Boundary Conditions

The parabolic marching technique used for the solution of the vorticity transport equation requires the knowledge of the initial conditions on vorticity and velocity at the starting face of Box 1 (see fig. 2.1) and the boundary conditions on the rectangular boundary of each subsequent cross-flow plane (see fig. 2.2).

The following procedure is employed to establish the initial conditions. The viscous box solution is started at the first face of the first box with the potential flow velocity field resolved into the box coordinates, the boundary layer vorticity that feeds into the box, and a lamb vortex of low strength placed at a location compatible with the potential flow solution. Holding the boundary layer input of vorticity and the velocity values at the boundary constant, the solution is advanced using small Δx values for a few stations. This is continued until (a) a feeding sheet of vorticity connects the boundary layer vorticity to the Lamb vortex, and (b) the total vortex strength becomes equal to the vortex strength employed in the potential flow model. When these conditions are met, the solution obtained for velocity and vorticity are assigned back to the starting face as the required starting conditions.

As was pointed out in Section 2, the extension of the box boundaries beyond the leading edge offers possibilities of significantly improving the way in which the local boundary conditions are imposed (see figure 2.2). The extended region of the no-slip surface permits an accurate positioning of the boundary layer vorticity input points, limited only by the grid size of box program in relation to the boundary layer thickness. If a clustering transformation technique is used, the cross-plane geometry would even facilitate the boundary layer vorticity profile to be exactly incorporated at the box boundary. At this stage, however, no grid transformation technique is used and the vast difference between the grid sizes of the viscous box and the boundary layer program necessitates certain approximations. Essentially, all the boundary layer vorticity is now placed at one point at the box boundary while keeping total circulation to be same between two cases. The details of interpreting the boundary layer results compatible

with the box grid size were discussed earlier in Section 4. On the no-slip boundary of the box, velocity is specified as zero and the vorticity is determined using finite differences. The vorticity values are set to zero on the free edges of the box and the velocities are obtained by resolving the potential flow velocities into the box coordinates.

5.3 Modifications to Finite Difference Technique

Previously, the vorticity box program employed up-wind differencing for the in-plane derivatives of vorticity while solving the vorticity transport equation, (5.1). The advantages (not being stability limited by cell Reynolds number, being able to preserve "transportive property") and disadvantages (lower-order formal accuracy, numerical viscosity) of this difference scheme are well documented in open literature (see for example, ref. 18). Whether the numerical diffusion introduced by the upwind differencing can be tolerated or not depends to a large extent on the physics of the problem. In the studies of vortex growth or decay in a viscous medium, errors due to numerical viscosity become critically important.

In view of the importance of understanding the errors due to numerical viscosity, an extensive study of error analysis was undertaken at private expense and the results may be found documented in reference 19. This analysis involves the study of a Lamb vortex positioned axially in a viscous stream, for which case an exact analytical solution is available. As shown in figure 5.1, the fully upwind differencing scheme causes the vortex to decay very rapidly in comparison to the exact solution. It was also found (ref. 19) that a differencing scheme like central differencing, which is a higher-order accurate scheme and which is also free from numerical viscosity for the present form of governing equation, gives rise to "wiggles" in the solution near the boundaries. Thus, a tradeoff is apparent and a combined central/upwind differencing is found to give the best result (fig. 5.1). Under the new scheme, at a given grid point either the central or upwind differencing is used depending upon the value of a parameter, ϕ, defined by

$$\phi = \xi \, \Delta y \cdot \Delta z \cdot Re$$

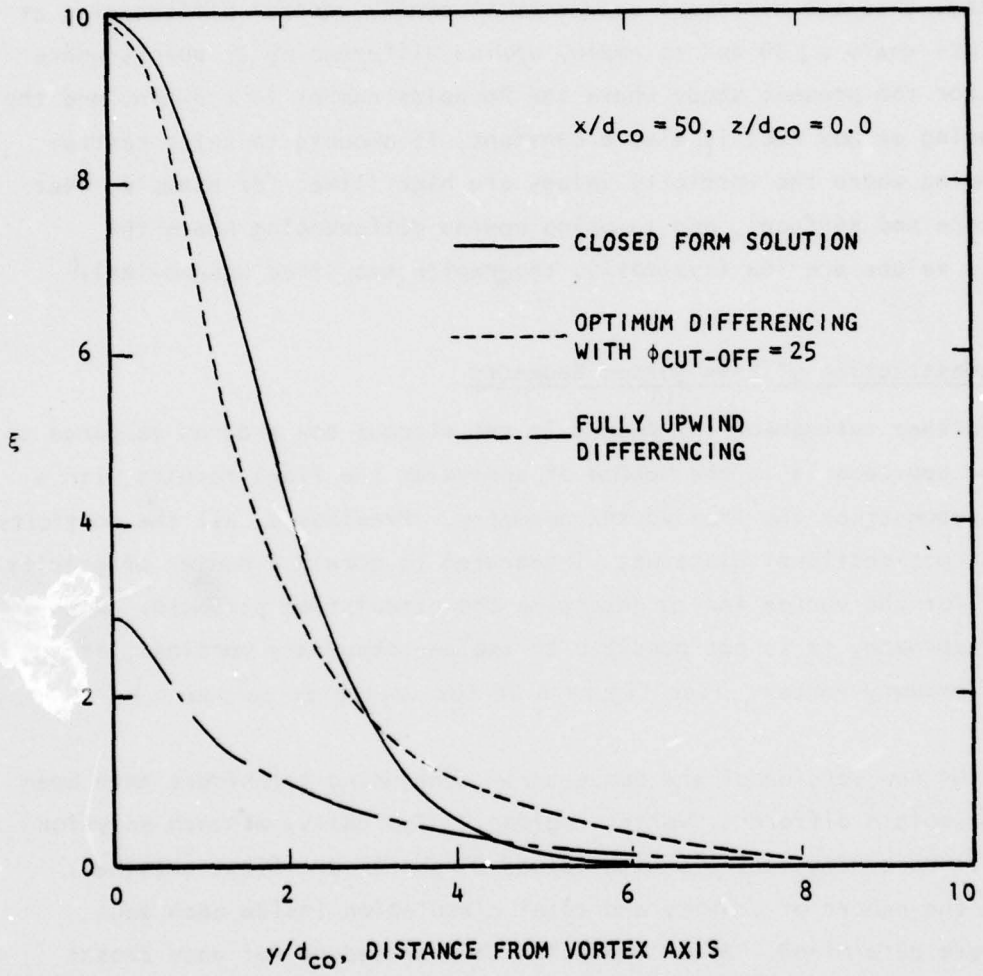

Figure 5.1 Effect of Differencing Scheme on the Diffusion of a Lamb Vortex

where ξ is the local vorticity value and Re is the flow Reynolds number. Upon studying the effects of various grid spacings and the flow Reynolds number on the errors for the ideal Lamb vortex case, the optimum value of ϕ has been found to be in the range $25 \leq \phi \leq 50$. If one chooses a value of $\phi = 30$, say, then the numerical scheme is to employ central differencing at grid points where $\phi \geq 30$ and to employ upwind differencing at points where $\phi \leq 30$. For the present study where the Reynolds number is constant and the grid spacing at box face is also a constant, it amounts to using central differencing where the vorticity values are high (like, for example, near vortex core and surface), and to using upwind differencing where the vorticity values are low (typically, the region near free boundaries).

5.4 Reconstruction of Free Vortex Geometry

A further refinement introduced in the viscous box program compared to the prior approach is in the method of analyzing the final results with a view to reconstruct the free vortex geometry. Previously, all the vorticity in each cross-sectional plane was integrated to obtain a center of gravity position for the vortex and to determine the circulation strength. With such an approach, it is not possible to isolate secondary vortices, if any, from the primary vortex. (See figure 6.20 for vorticity contours.)

In the new version of the box program contouring techniques have been added to isolate different "vortex regions." Typically, at each solution plane, all vorticity contours with values 0^+ and 0^- are first obtained, and then the center of gravity and total circulation inside each such contour are determined. After repeating this procedure for each cross-sectional plane, vortex filament geometry and variation of the circulation strength along its length are readily reconstructed. At the end of this procedure the vortex geometry definition will be in box coordinates. These are then transformed to Hess coordinates using appropriate transformation relation.

6.0 PROGRAM INTERFACING AND SAMPLE CALCULATIONS

While developing the integrated computational program, some valuable operating experience was gained. In the material that follows, the efforts are applied to a 65° delta wing as described in Section 6.1. The efforts are presented in cases having one or more cycles. A case is defined as a consistent run through all the necessary cycles without changing the method. A cycle is defined as one complete run through all the programs as shown on the chart in Section 2.0 with the end being pressures and forces from the potential flow model. Four cases have been run but only the last has been consistent through each of its three cycles. In each of the earlier cases, the operating experience suggested a major improvement to the technique, and it was deemed appropriate to start anew rather than to continue with additional cycles. The following table describes the cases studied.

TABLE 1

OPERATING EXPERIENCE

Case	Description	Cycles	Results
1	Initial estimate of free vortex strength high by factor 2.35	2	Unrealistic pressures and vortex growth
2	Initial estimate of Case 1 reduced by $\frac{1}{2}$	1	Vortex growth similar to Case 1; Boundary layer input too high
3	Boundary layer vorticity reduced to that between $\delta - \delta^*$; Initial conditions same as Case 2	1	Vortex growth and position qualitatively good; Box starting conditions in error
4	Boundary layer rate of circulation input reduced by rate of leaving the box; Starting conditions of box corrected; Case 2 initial conditions	3	Boundary layer vorticity correct only for potential flow with no free vortex; Must converge on free vortex position and strength before changing boundary layer; Vortex position must be represented more accurately

The first three cases are discussed in Section 6.2. They are presented in this report primarily to illustrate the importance of some of the parameters. Also the experience gained in evolving correct operating procedures will assist future operators of the program.

Case 4, which incorporates all improvements as learned from the previous case is discussed in Section 6.3.

During the analysis of Cases 1 through 3, it was found that an evaluation of the cross-flow velocity ($\bar{v} \times \bar{\omega}$) at the free vortex axis with the potential flow program would enhance convergence. This is discussed in Section 6.2.1.

6.1 Model Description

In order to develop the techniques of this hybrid potential/viscous flow model, a 65° delta wing with rounded leading edges was selected for application. This wing is similar to one tested by Henderson (ref. 16) except for a small trailing edge extension on his wing. The reasons for selecting this wing are: (1) both sharp and rounded leading edge data are available for overall forces and (2) the wing is thin enough to insure that a leading edge vortex is formed at a relatively low angle of attack. An angle of 14° was selected for analysis to insure a high enough angle to have vortex formation over the entire leading edge but not too high to cause bursting over the wing.

The airfoil selected for the 65° delta was chosen to be similar to that of Henderson's primarily near the leading edge. The streamwise section is a NACA 0006 airfoil reduced to a t/c of 0.02302. It is further modified from 5% of x/c to the leading edge to correspond to the largest leading edge radius configuration of Henderson's wing. The first 0.816% of the leading edge is shown in figure 6.1. From 0.816% to 5.0%, there is a straight line fairing into the reduced thickness 0006 airfoil. The airfoil is maintained constant from root to tip, and since the tip has zero dimensions the outboard stations become very thin.

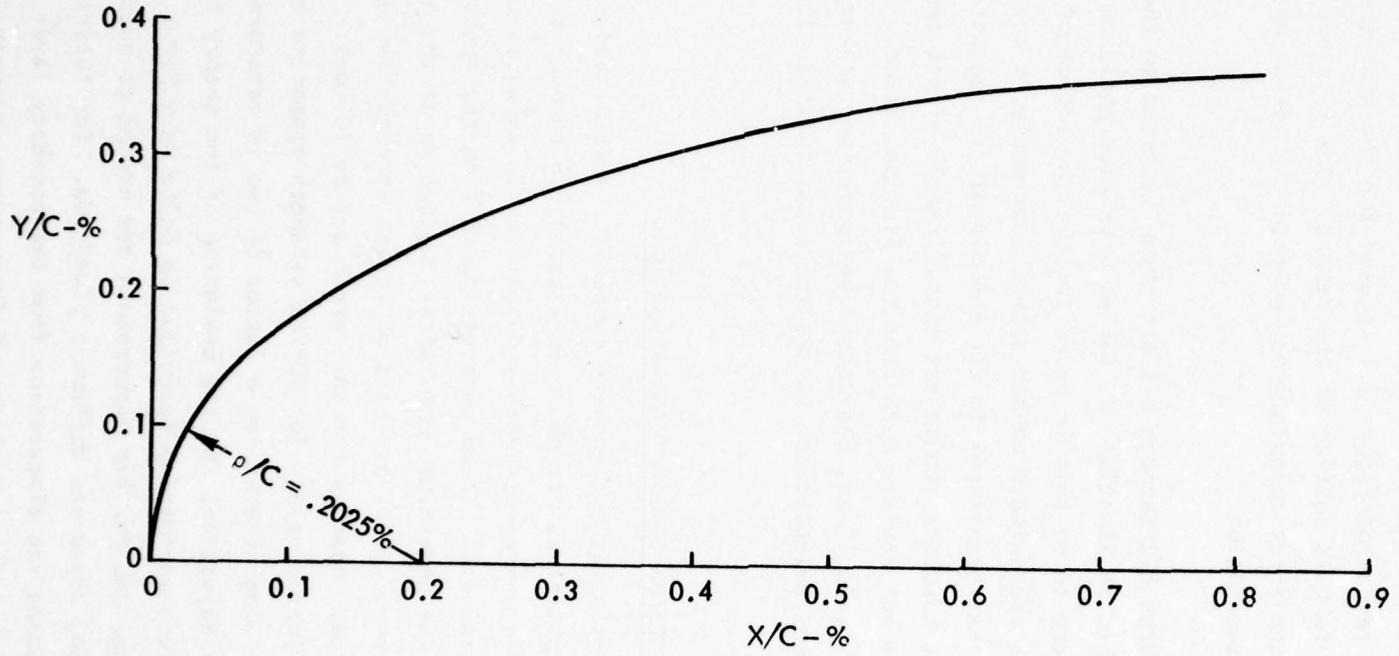

Figure 6.1. Streamwise Section Leading Edge Shape - t/c = 0.02302

These thin airfoils made it necessary to have the viscous box configuration extended beyond the leading edge as shown in figures 6.2 through 6.5. The face and end of each box as shown on the wing in figure 2.1 are illustrated. The box layout of figure 2.1 is used for the analysis and the results are presented in this section of the report. Box 1 is not used in the analysis because the first calculations indicate the vortex has not formed, i.e. no flow separation.

The boxes of figures 6.2 through 6.5 are shown inclined to the wing reference plane and this inclination, ε, varies with each position of the boxes. It was necessary to do this in order to have the bottom of the box fit the airfoil in the approximate manner shown. Obviously, a coordinate system for the boxes that transforms to fit the airfoil is suggested. The compromise shown here, however, should not significantly affect the data since the airfoil does not deviate much from the flat box floor. In computing the boundary velocities, the actual box positions are used; however, the viscous box calculations ignore the small twist in the boxes caused by the varying ε.

6.2 Results of First Three Cases of Investigations

In Case 1 two consistent cycles were computed. Initial and resulting vortex strengths and positions are shown in figures 6.6 through 6.8. The original estimated free vortex strength and position is shown as the dashed lines in figures 6.6 and 6.8. These were estimated from the method reported in reference 11. It was determined only after two cycles of the program were completed that the original estimate of vortex strength was about 2.35 times its correct value. Reasons for this error are as follows: First, the theoretically estimated values for vortex strength appear to be the sum for both sides of the wing, therefore, a factor of two is determined. Then, the 0.35 factor is an adjustment for the deviation of the theory from experiment. *Note: This estimating technique is valid only for a class of sharp edge delta wings, and further corrections are needed to estimate the effect of round leading edges and different planforms.* For future applications a new method, using the circulation from the boundary layer, is being developed to obtain the initial estimate of free vortex strength.

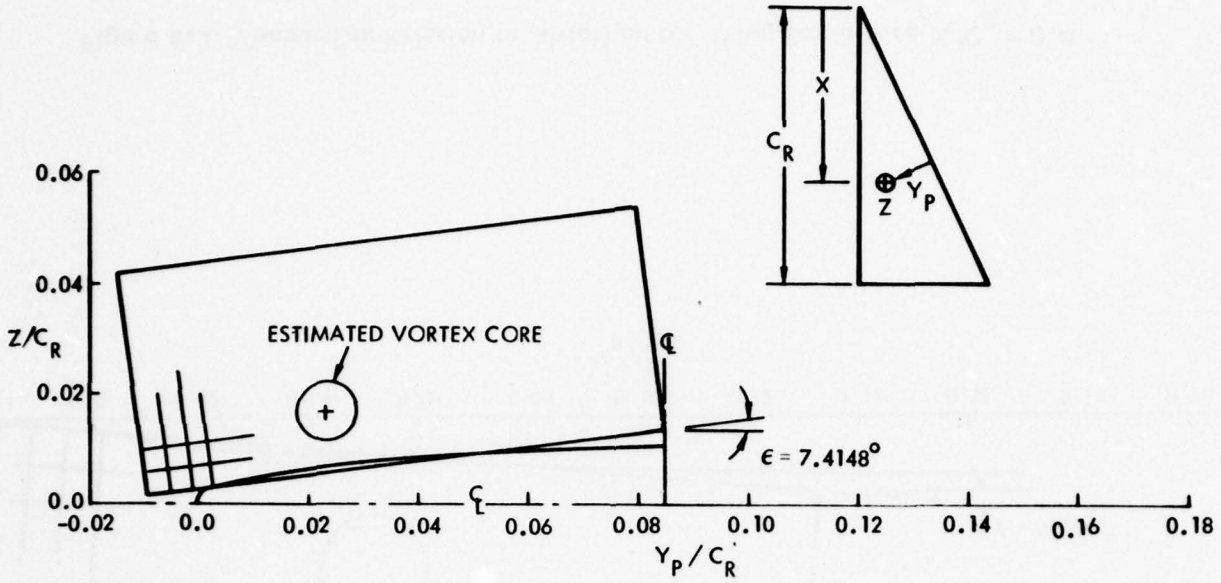

Figure 6.2. Viscous Box Relation to Airfoil on 65° Wing, Box 2 Face, $X/C_R = 0.2$

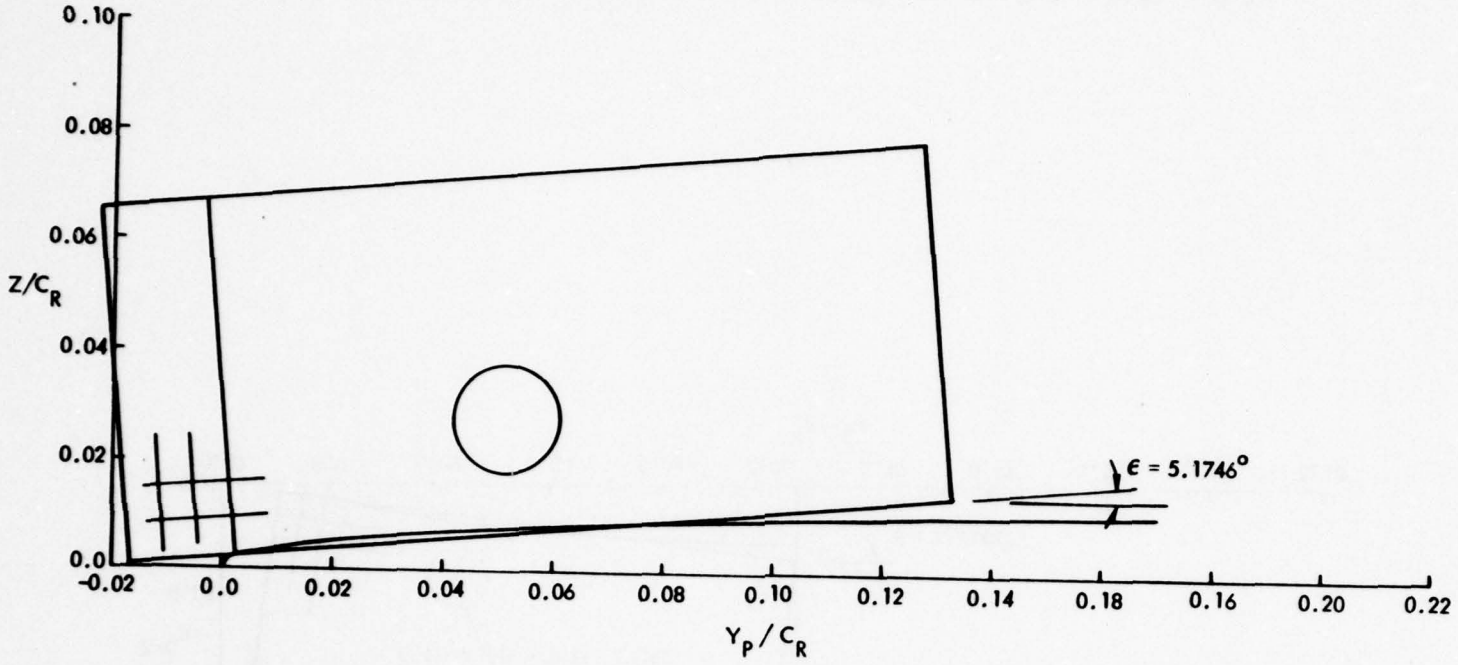

Figure 6.3. Viscous Box Relation to Airfoil on 65° Wing, Box 3 Face, $X/C_R = 0.4$

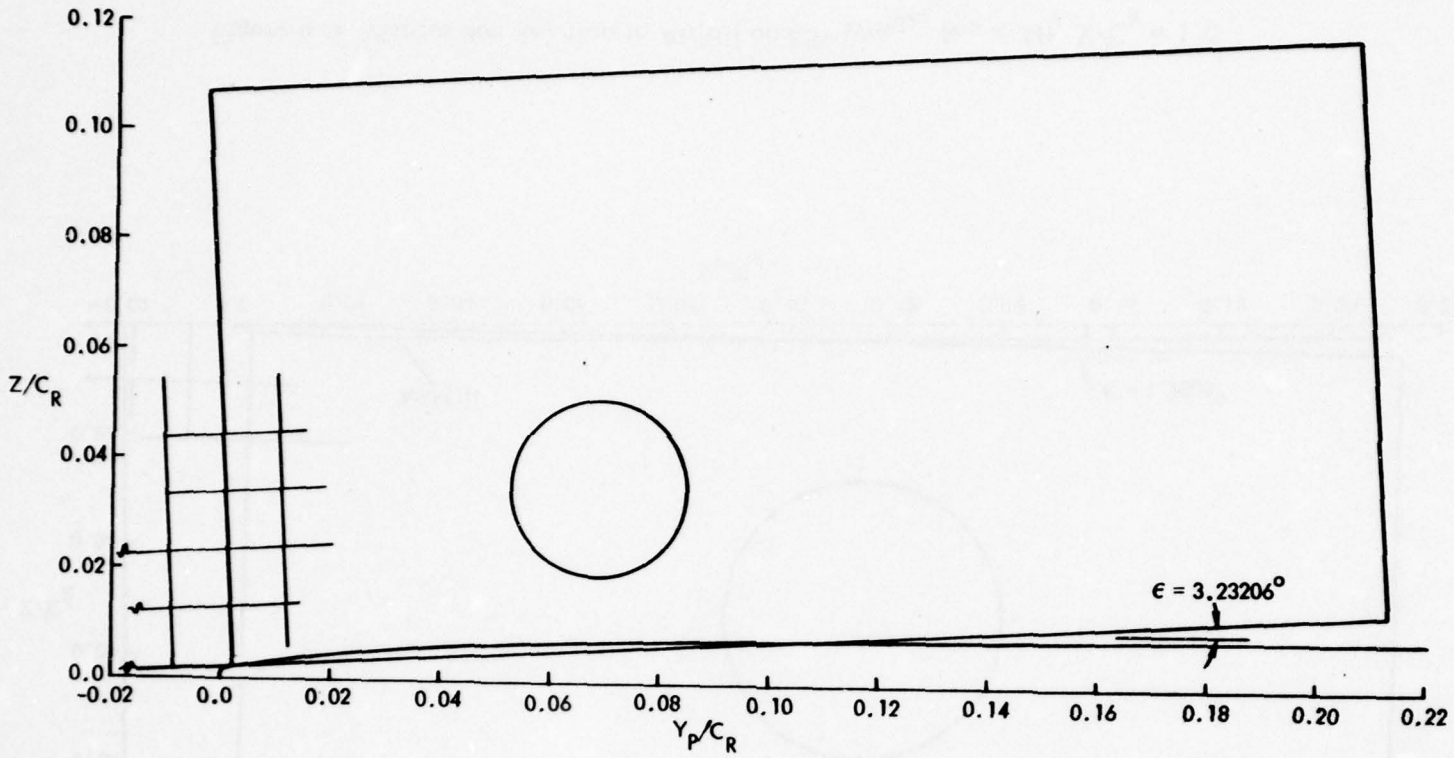

Figure 6.4. Viscous Box Relation to Airfoil on 65° Wing, Box 4 Face, $X/C_R = 0.6$

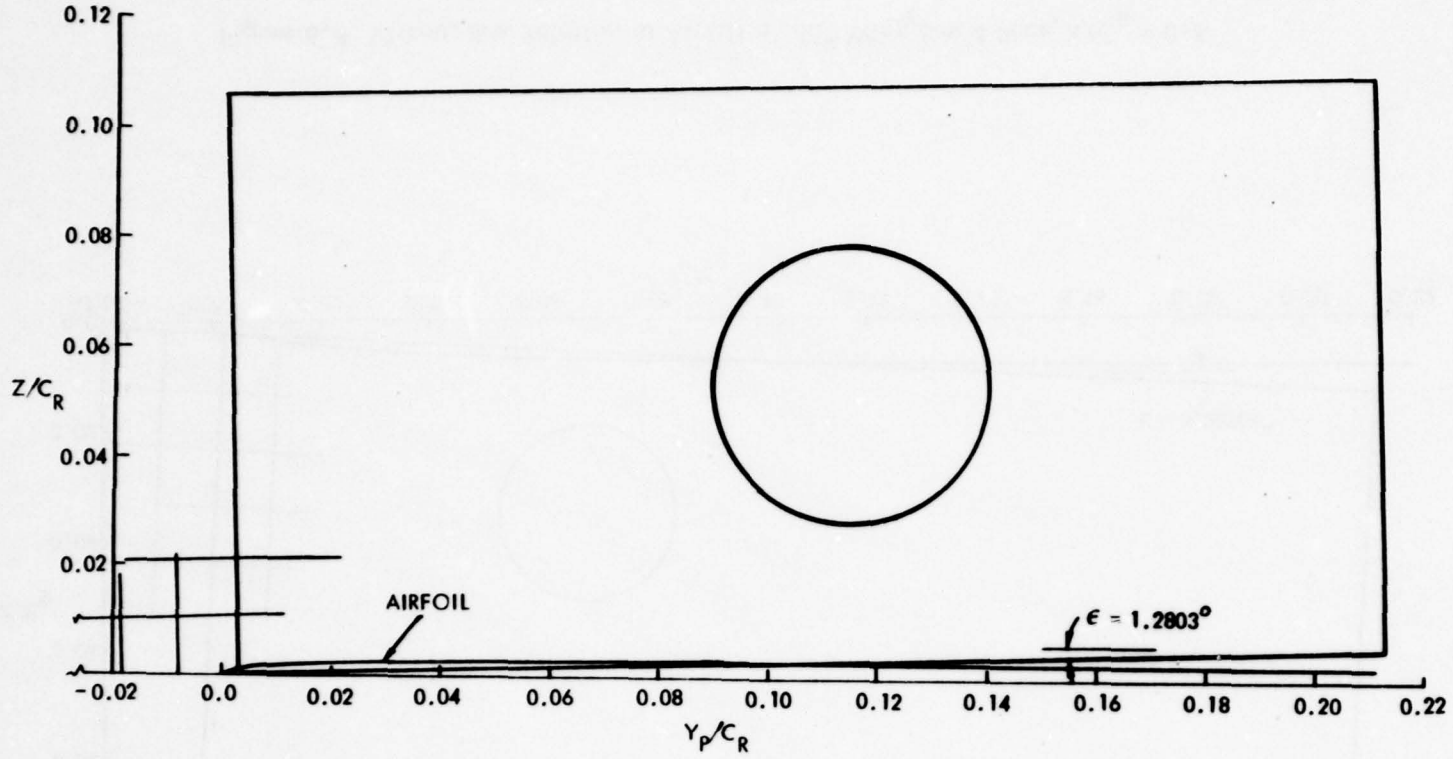

Figure 6.5. Viscous Box Relation to Airfoil on 65° Wing, Box 4 Aft, $X/C_R = 1.0$

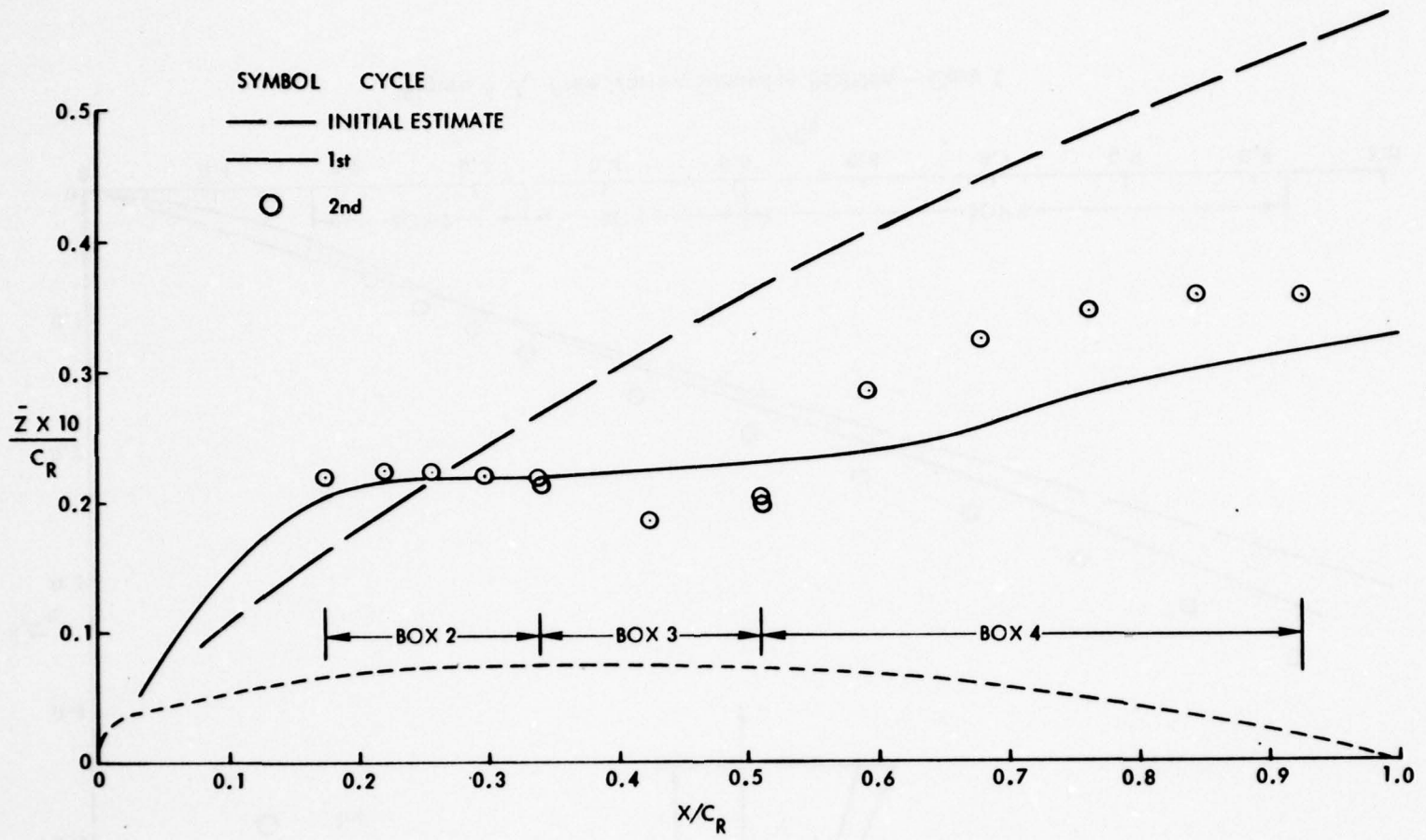

Figure 6.6. Free Vortex Vertical Position - Case 1

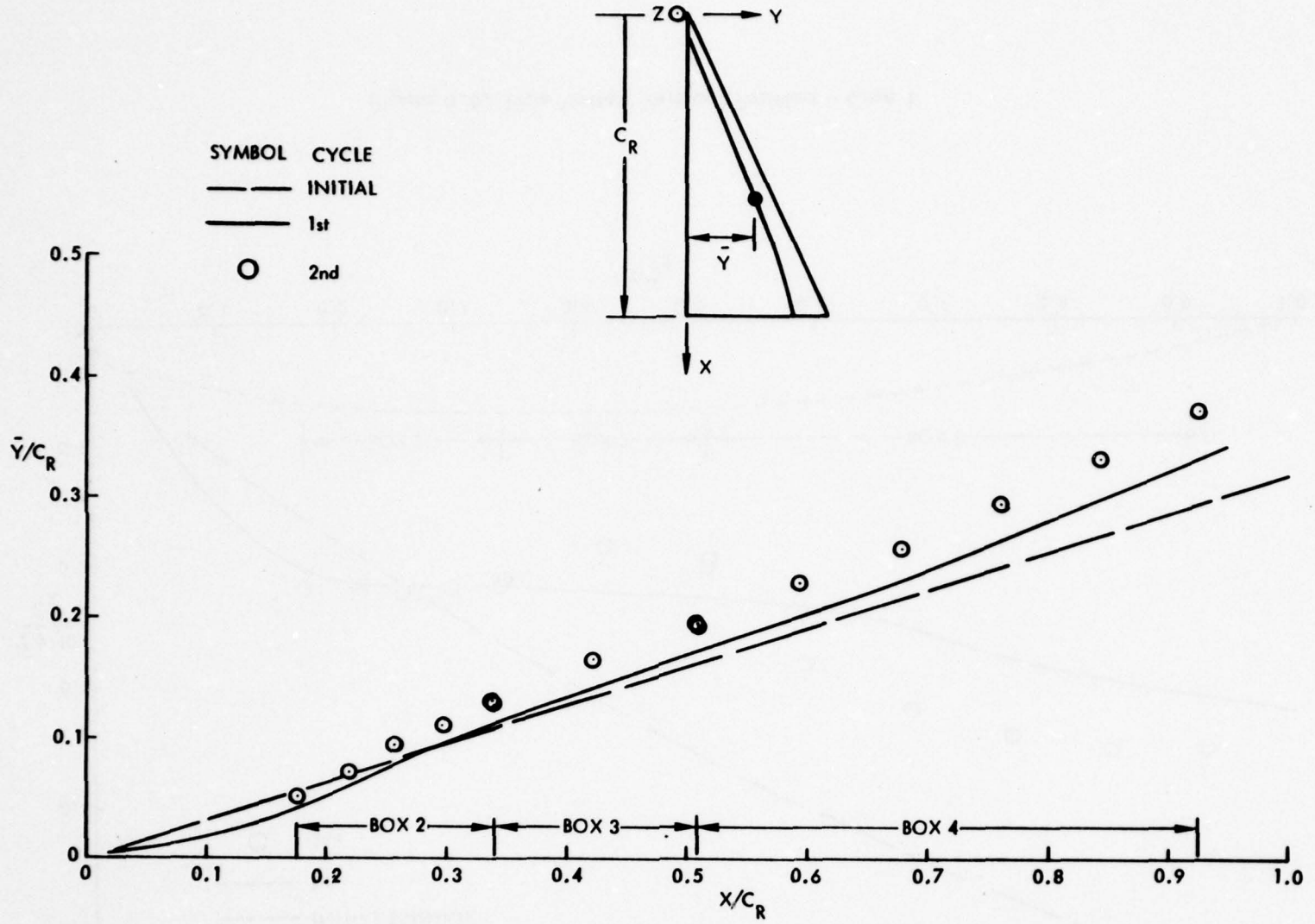

Figure 6.7 Free Vortex Spanwise Position - Case 1

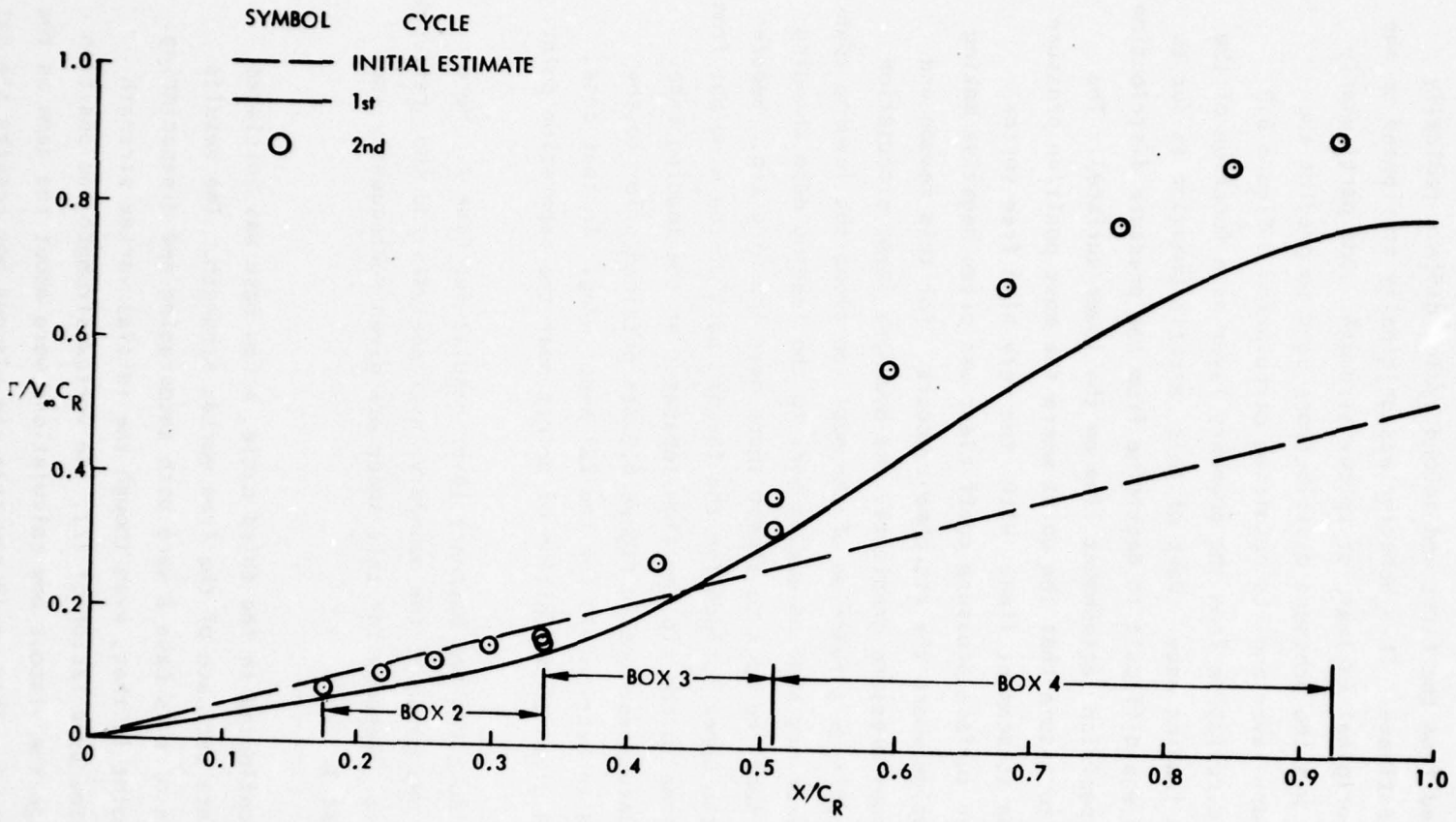

Figure 6.8. Free Vortex Strength - Case 1

As noted in figures 6.6 and 6.8, the vortex strength and vertical height as determined from the first and second cycles differs radically from the original estimate. This behavior was originally attributed to the highly inaccurate original estimate of vortex strength. One particularly significant effect was the pressure distributions used to predict the leading edge boundary layer and its resulting circulation. Figure 6.9 shows the erratic circulation from the boundary layer as a function of the position along the leading edge. Part of this erratic behavior is due to the pressures. It was difficult to determine from the pressure distribution a proper starting position (attachment line on the lower surface). The criteria used was to assume that the point where the most positive pressure occurred was on the attachment line. With the very high free vortex strength, the lower surface pressure coefficient was often negative making it difficult to decide where the attachment occurs. For this reason and the resulting unusual pressure gradients, the boundary layer circulation prediction was erratic as a function of the position along the leading edge. This strange behavior may also be due in part to the leading edge changing from very rounded near the apex to almost sharp near the wing tip. Separation occurred on the upper surface for the forward part of the wing but from about 50% of the span to the tip the flow separates at the leading edge. Furthermore, the data presented in figure 6.9 was obtained prior to the analysis described in Section 4.0 for the 22° swept wing. In that case, more attention was given to definition of points near the separation point.

Figure 6.9 also gives the boundary layer results for Case 2. Here careful attention was given to the boundary layer analysis and the pressures were more realistic. Reasons for this shape are given subsequently when comparing with Case 3.

Instead of continuing to the third cycle, a new case was initiated with a more accurate estimate of the free vortex strength. The results of the first cycle of this Case 2 were both encouraging and disappointing. The encouraging point is that, even though the initial vortex strength estimate was reduced by a factor of 1/2, the vortex strength and position after going through the viscous box calculations were about the same as the first cycle of Case 1. This would say that the viscous box results are not

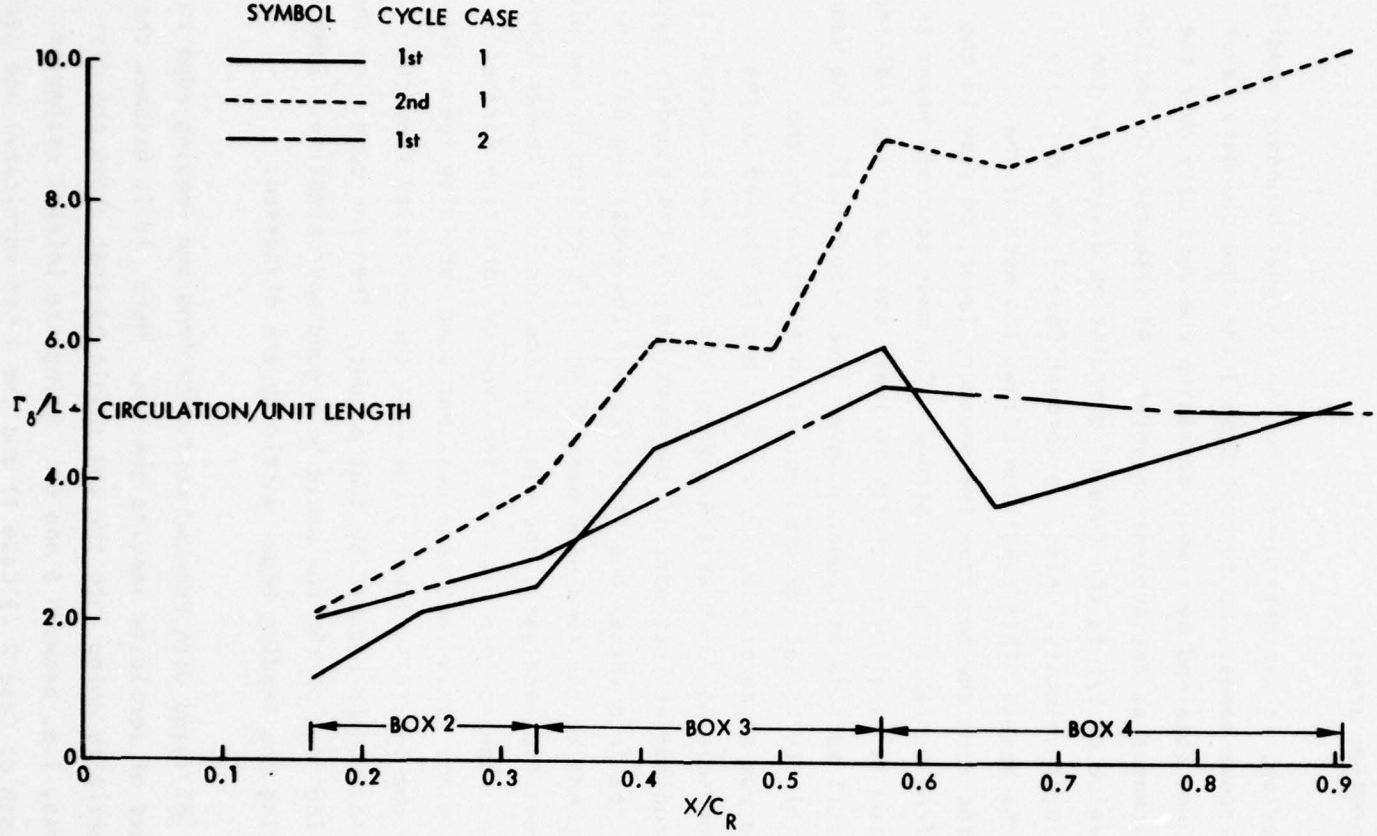

Figure 6.9. Spanwise Boundary Layer Circulator - Case 1 & 2

are not strongly affected by the initial vortex strength. Of course, the discouraging fact was that the box results were just as radically different from the original estimated values as that for Case 1. It was then necessary to examine other problem areas.

After some review, it was determined that an improper boundary condition was set for the viscous boxes. Up through Case 3 the shed boundary layer circulation, Γ/L, was obtained by simply averaging the vorticity over the boundary layer thickness at the separation point. As discussed in Section 4.4, the correct value of Γ/L is the rate of circulation divided by the average boundary layer velocity. Also, up through Case 3, no vorticity is allowed to leave the boxes. This condition allows too much of the vorticity, being fed into the box from the boundary layer, to stay in the box; causing the free vortex to be too strong. The most accurate means to correct this problem is to allow vorticity to leave the box at its trailing edge near the airfoil surface as boundary layer (see figure 2.2). One means of accomplishing this is to set the gradient of vorticity along the z-direction of the box to zero; i.e. $\partial\bar{\omega}/\partial z = 0$. This is opposed to the current practice of setting $\bar{\omega} = 0$ at the edge of the box. This concept is equivalent to acknoqledging that part of the vorticity in the boundary layer goes into forming the free vortex and its lift, and the remaining part is that which corresponds to the remaining part of the lift created by the wing surface. In viscous flow analysis, the wing surface vorticity leaves along the entire trailing edge to join with the free vortex vorticity further downstream of the wing. This fact requires that some vorticity leave the box. If one knew the vorticity leaving the box, the vorticity from the leading edge could then be reduced by that amount. Then the condition that $\omega = 0$ at the trailing edge of the box would be a good approximation. Some attempts at reducing the leading edge vorticity are discussed.

Case 3 was initiated with reduced vorticity from the leading edge to simulate the effect of vorticity leaving the box. Here, it is assumed that the portion of vorticity going into the box should be that above the displacement thickness, i.e. between δ and δ^*. Using the initial estimated free vortex strength of Case 2 ($\frac{1}{2}$ Case 1) and the $\delta - \delta^*$ vorticity, one cycle

of the program was run as Case 3. The circulation or vorticity obtained from the boundary layer for the two cases is presented in figure 6.10.

Behavior of the shedding circulation as a function of X/CR is strange, but informative. Upon investigation it was determined that up to the high point at box 4 face, turbulence occurs before separation. The remaining points have laminar separation. This causes some of the strange behavior, but most of the variation in circulation as shown from the Γ_δ line is due to the relation of local angle of attack and leading edge radius. Circulation increases along the leading edge initially due to increasing local angle of attack and reduction in the leading edge radius. Continuing along the leading edge, the separation moves forward to an optimum position from the leading edge, (i.e. peak vorticity). After this, the radius gets so small that the separation rapidly approaches the leading edge where the vorticity gets smaller because turbulent flow has not developed and the limiting condition of a sharp leading edge has been obtained.

The information gained from this test of reduced leading edge vorticity is important. The level and shape of circulation obtained from the boundary layer is quite different for Cases 2 and 3. No other difference occurs between these two cases, but the resulting free vortex strength and position is significantly different as shown in figures 6.11 through 6.13. In each figure the results look qualitatively better for Case 3. The only real conclusion though is that the boundary layer vorticity is an extremely critical parameter. Careful attention must be given to computing this parameter. First, the airfoil shape and pressure distributions must be obtained accurately, and second, the circulation rate should be used to obtain the shed leading edge circulation (vorticity), and finally, the boundary conditions on the viscous box must provide for the proper vorticity leaving the box as well as entering it.

An alternate method of obtaining the rate of circulation leaving the box is used for Case 4 and suggested for later application. It is assumed that the wing surface velocity at the inboard box boundary, as calculated from the potential flow programs, can be used to compute the existing rate of circulation vector, i.e.

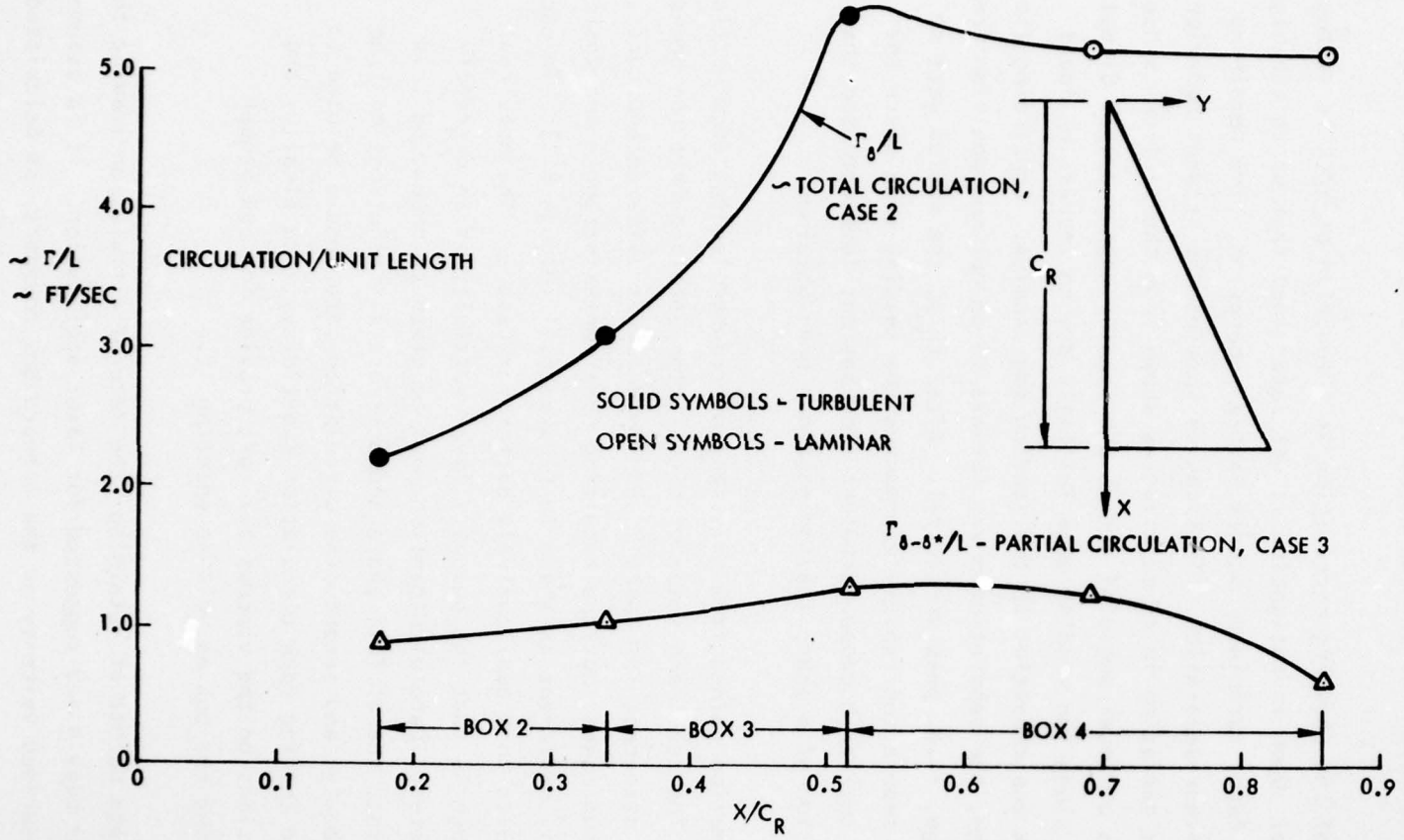

Figure 6.10. Spanwise Boundary Layer Circulation

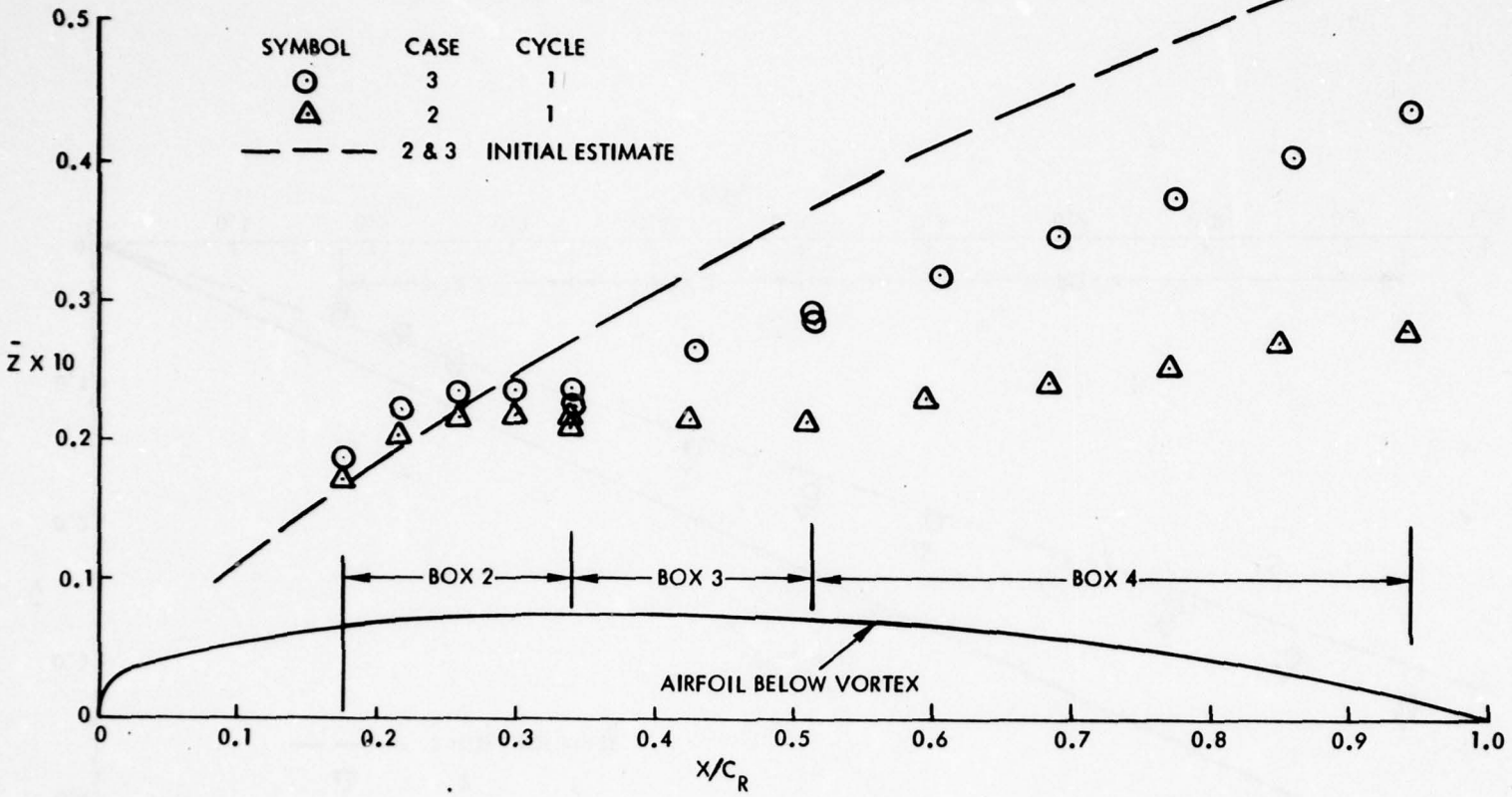

Figure 6.11, Free Vortex Vertical Position Cases 2 & 3

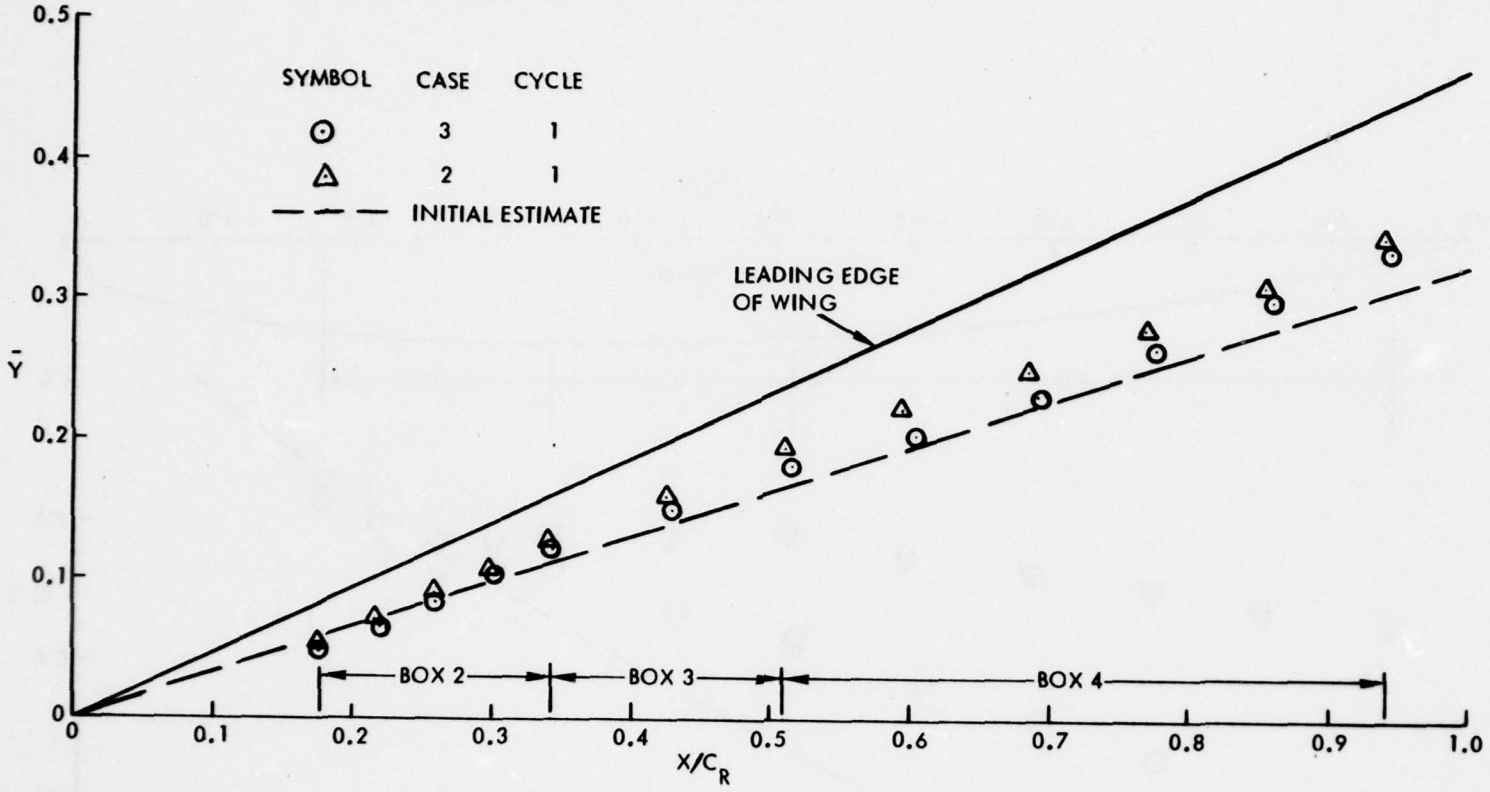

Figure 6.12_ Free Vortex Spanwise Position Cases 2 & 3

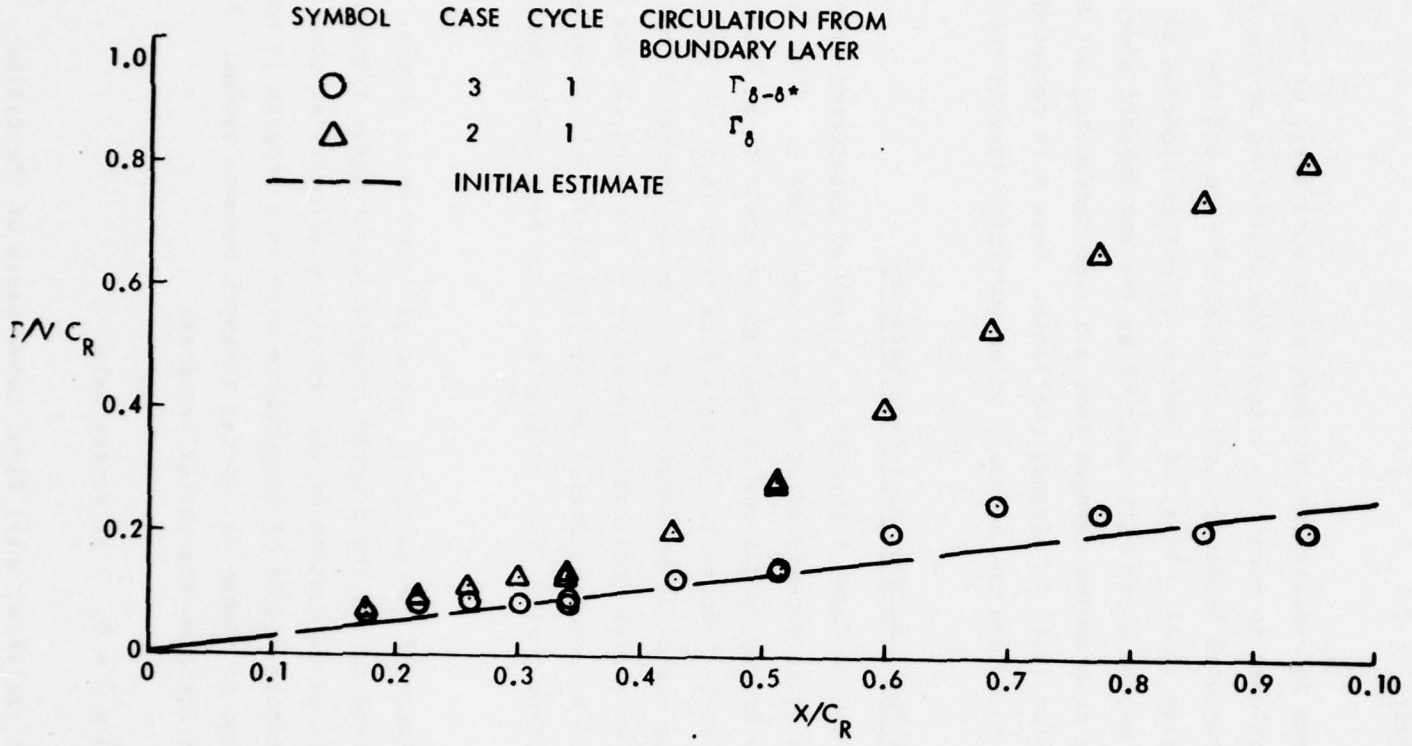

Figure 6.13. Free Vortex Strength - Cases 2 & 3

$$\left(\frac{d\vec{r}}{dt}\right)_o = \frac{w_{pot}^2}{2}\,\vec{i} - \frac{u_{pot}^2}{2}\,\vec{k} \qquad (6.1)$$

This rate could be used to compute the boundary value vorticity, or the net rate of circulation allowed to enter the viscous box could then be the difference between the computed boundary layer circulation rate and the assumed rate of equation (6.1). This, of course, is not as rigorous as the previously suggested method which sets $\partial\omega/\partial z = 0$ at the box inboard side. The latter will take some programming changes that are time consuming, but the information for equation (6.1) is already available. Case 4 is computed using equation (6.1) to obtain the boundary value vorticity leaving the box.

6.2.1 Initial Vortex Position and Cross-Flow Velocity

In the computations of Cases 1 through 3, a problem associated with vortex position was discovered only after going through Case 3. This was a problem causing the starting conditions at the face of box 2 to be incorrect at the face of box 2 to be incorrect. At this face there is provision to allow the initial free vortex to be input in its three orthogonal directions. In the process the free vortex inclination relative to the wing surface was too much. This caused a large distortion of the flow field velocities and errors for all the other boxes. This problem has also been corrected for Case 4.

The initial estimate of vortex position can be improved by another technique, which evolved during the program interfacing of Cases 1 through 3. This is related to an evaluation of the cross-flow velocity at the vortex axis. The ultimate result of convergence with this program is no force on the vortex and no change in vortex strength between cycles. In mathematical terms no force on the vortex requires:

$$\bar{V} \times \bar{\omega} = 0, \qquad \text{at vortex axis.} \qquad (6.2)$$

Equation (6.2) is not satisfied until final convergence of the cycles; therefore, neither the pressures nor forces calculated by the potential flow

model are correct until convergence. This is shown by examination of the integral equation of motion for steady flow and negligible body forces;

$$\bar{V} \times \bar{\omega} = \nabla\left(\frac{V^2}{2} + \int \frac{dP}{\rho}\right), \tag{6.3}$$

With circulation (free vortex) in the flow field having a net force ($\bar{V} \times W \neq 0$), the Bernoulli equation for pressures in irrotational flow is no longer valid. This causes the preconvergent pressure integration technique of the AIP program to give erroneous forces.

As was noted previously, if very large errors are present in the estimated free vortex strength and position, the pressures and interference effects between wing and vortex are largely in error. To avoid this problem before going through all the viscous analyses, a check on $\bar{V} \times \bar{\omega}$ should be made with the potential flow program and the vortex position changed accordingly. Figure 6.14 illustrates such an analysis. The velocity normal to the vortex axis and parallel to the wing reference plane is given as a function of the X/C_R. Results from the initial position of vortex in Case 1 indicate the vortex wants to move vertically from the surface near the apex and towards the surface as the vortex moves to the wing trailing edge. If this tendency had been relieved by moving the vortex in its desired direction prior to going through the viscous analyses, the new starting conditions for the viscous analyses would have been more compatible. This was not done and figure 6.6 shows the viscous box results did move the vortex in the directions indicated by the $\bar{V} \times \bar{\omega}$ analysis. However, because of the extremely oversized estimate of vortex strength and the other inaccurate conditions mentioned in Section 6.2, the viscous box overshot the positions required by the potential flow model. The results of the potential flow $\bar{V} \times \bar{\omega}$ analysis for the end of cycle 1 are also shown in figure 6.14. The increase in vortex height near the apex did relieve the force on the vortex some but the high vortex strength produced by the box results at the outboard part of the wing caused even more discrepancy in the vortex position. A part of this discrepancy in the box 3 and 4 results is due to inaccurate starting conditions in box 2. The cycle 2 vortex position shown in figure 6.6 shows an encouraging move of the vortex back

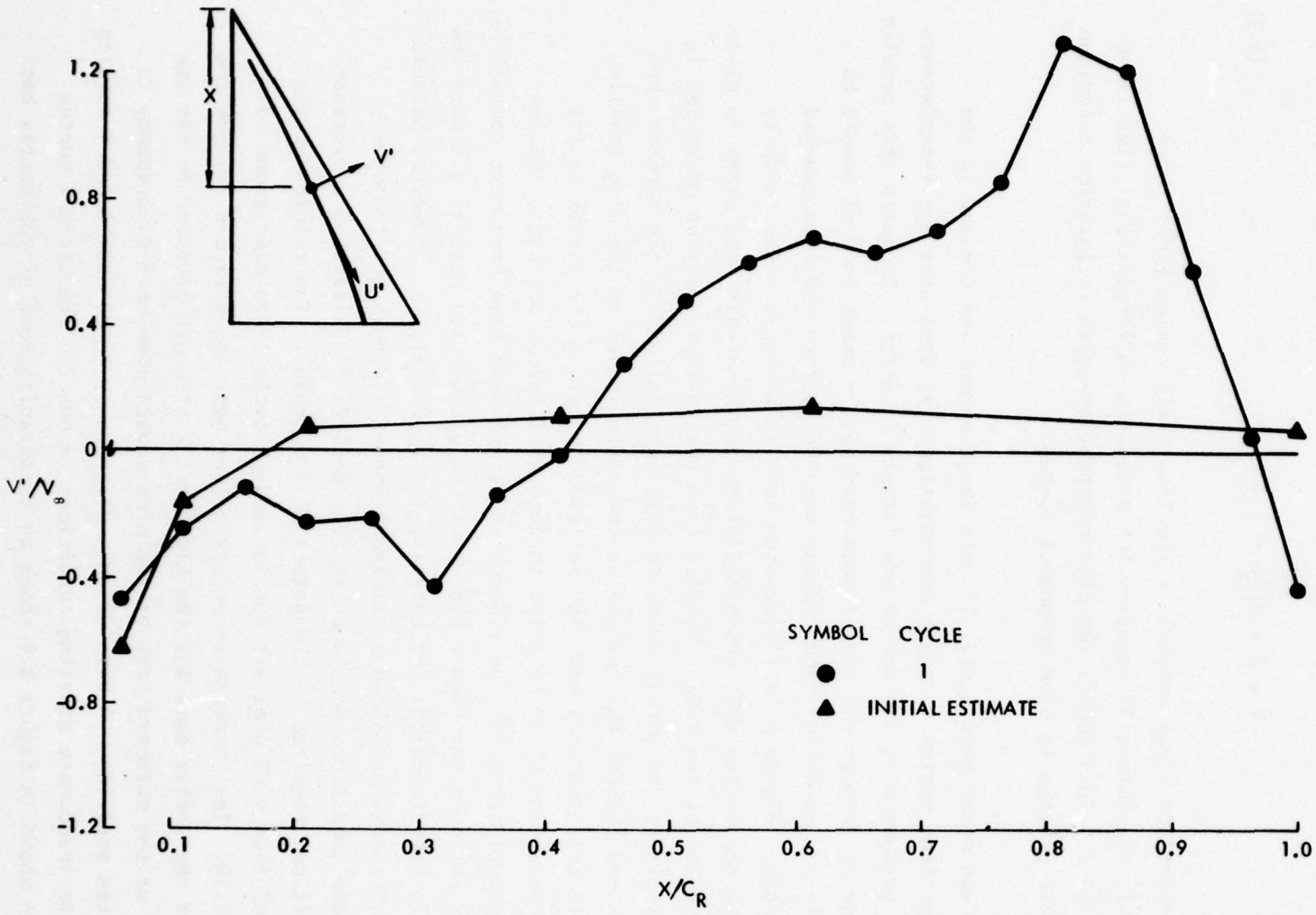

Figure 6.14. Cross Flow Velocity at Free Vortex

towards the initial position in the box 4 area. Unfortunately with so many problems this case was instructive but would probably never converge.

The check on $\bar{V} \times \bar{\omega}$ is applied after potential flow runs in Case 4. This loop in the program hopefully would have the effect of approximating a more accurate vortex position for a constant vortex strength. The strength and position is then varied by the viscous box portion of the cycle. Unfortunately in Case 4 the vortex was moved in the wrong direction. Further investigation is required before this technique can be used successfully.

6.3 Case 4 - Incorporation of Program Corrections Developed in Cases 1 through 3

The techniques learned in Cases 1 through 3 and applied in Case 4 are as follows:

- Apply improved original estimate of free vortex strength.
- Check for $\bar{V} \times \bar{\omega} = 0$ at the free vortex after each potential flow run to improve convergence.
- Maintain turbulent boundary layer separation along entire leading edge.
- Maintain the rate of circulation coming from the leading edge rather than the absolute value of circulation per unit length.
- Compute the rate of circulation leaving the box from equation (6.1) and apply as boundary condition at inboard side of each box.
- Use average rate of circulation between two box X stations to account for boundary vorticity (circulation) entering between box stations.
- Apply correct vortex inclination at starting position of box 2.

Each of the above techniques were successfully applied to Case 4. Also, improvements were made in program operating procedures. All manual

operations were eliminated except evaluation of the boundary layer output and its input to the viscous box program. All potential flow runs were put into one run stream; that is, the Hess and vortex lattice programs were combined so that with an input of free vortex strength and position the output gives velocities at the box positions, pressures and leading edge for boundary layer, total force and moment coefficients, and surface pressures. This output is filed on the computer for access by the boundary layer and viscous box program. The potential flow program also checks the velocities at the free vortex axis and makes an adjustment in position of the vortex axis according to the cross-flow velocities, $\bar{V} \times \bar{\omega}$. This adjustment proved to be in error and needs further investigation before efforts subsequent to Case 4.

Results from Case 4 provided considerable insight to convergence techniques. Although Case 4 is not convergent in three cycles, the effort has provided the knowledge necessary to obtain convergence. The most significant error made in Case 4 is still in the application of the boundary layer output. The fact that surface pressures are not correct when $\bar{V} \times \bar{\omega} \neq 0$ cannot be ignored. The only conditions where the boundary output is correct is for the potential flow without a free vortex and for $\bar{V} \times \bar{\omega} = 0$ in the final converged cycle. As can be seen in figure 6.15, the boundary layer circulation shed into the viscous box increases for each cycle. This causes the total free vortex strength, figure 6.16 (as predicted by the viscous box), to increase with each cycle; i.e. a divergent condition. The only reasons for circulation from the boundary layer to increase with each cycle are: (1) the leading edge pressure increased due to $\bar{V} \times \bar{\omega} \neq 0$ and (2) probably the free vortex sheet, and secondary vortex need better definition in the potential flow model.

It is quite apparent now that the solution to the above problem is simply to relax the boundary layer input; that is maintain the boundary layer input from the potential flow without free vortex for all cycles until the vortex position and strength converges. Then the vortex sheet and secondary vortex can be defined more accurately resulting in accurate leading edge pressures which can be used in the boundary layer program to refine the shed vorticity. Current experience suggests that convergence

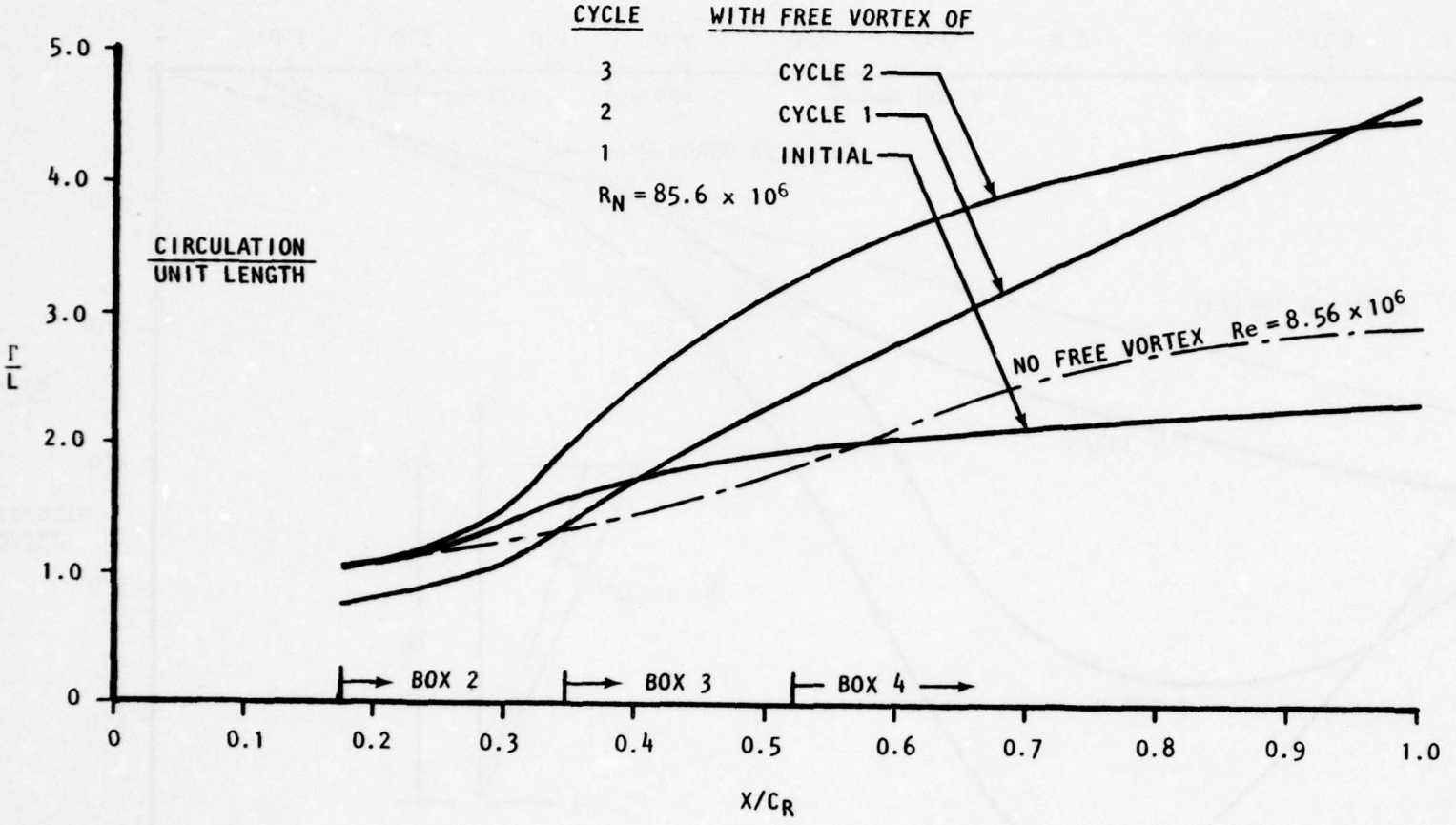

Figure 6.15 Boundary Layer Input to Viscous Box

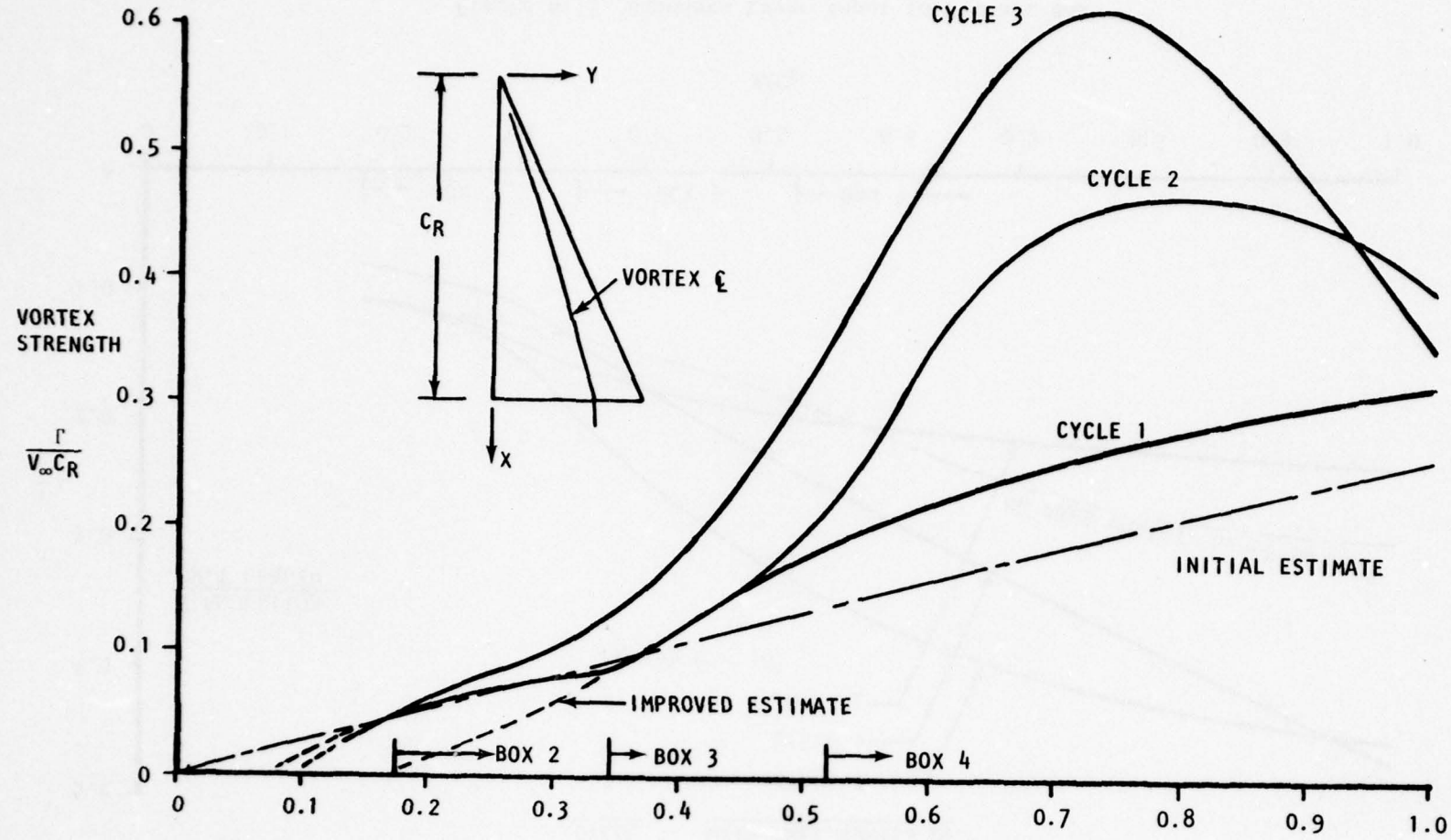

Figure 6.16 Vortex Strength Output From Viscous Box

will occur very rapidly for the first phase of above. In fact, it is conceivable that no manual interaction will be required in the computer as long as the boundary layer input is constant.

In spite of the lack of convergence, Case 4 did indicate very realistic output. When one considers the convection direction for vorticity shedding from the leading edge, figure 6.17, and the vortex position in figure 6.18, there is a realistic tendency for the vortex y-position to turn inward towards the root and z tends to go to zero near the beginning of box 2 (see line marked improved estimate). At the face of box 2 the convection direction (obtained from boundary layer output) is nearly parallel to the airfoil all the way to the root. Therefore, very little vortex height should be expected and then it should be near the root. Unfortunately, in all three cycles of Case 4, the vortex was restrained to the initial conditions at the face of box 2. It should have been allowed to relax to the "improved estimate" even for cycle 2. This could not easily be accomplished with the geometric restraints in the program.

The current program did not allow the vortex position to be defined accurately enough . Even though the vortex strength could be defined in twenty segments the vortex position could be defined in only four linear segments. This is an unnecessary restraint which can be removed. This restraint was also a problem when testing for $\bar{V} \times \bar{\omega} = 0$. It was found here that the overall lift coefficient and surface pressures were very sensitive to the vortex position and the desired accuracy could not be obtained with only four segments.

Another very realistic result is indicated with Case 4. The convection direction, θ, of the boundary layer vorticity is given for all cycles of Case 4 in figure 6.17. All of these boundary layer outputs are computed for a $R_N = 85.6 \times 10^6$. Also shown is the convection directions for $R_N = 85.6 \times 10^6$ and 8.56×10^6 for the boundary layer from the potential flow without a free vortex. All of these show large differences in convection direction. When comparing the dashed line at $R_N = 85.6 \times 10^6$ with those of Case 4 at the same R_N, it is easy to see that the large values of θ come from increasing the free vortex strength and this is not accurate as discussed earlier.

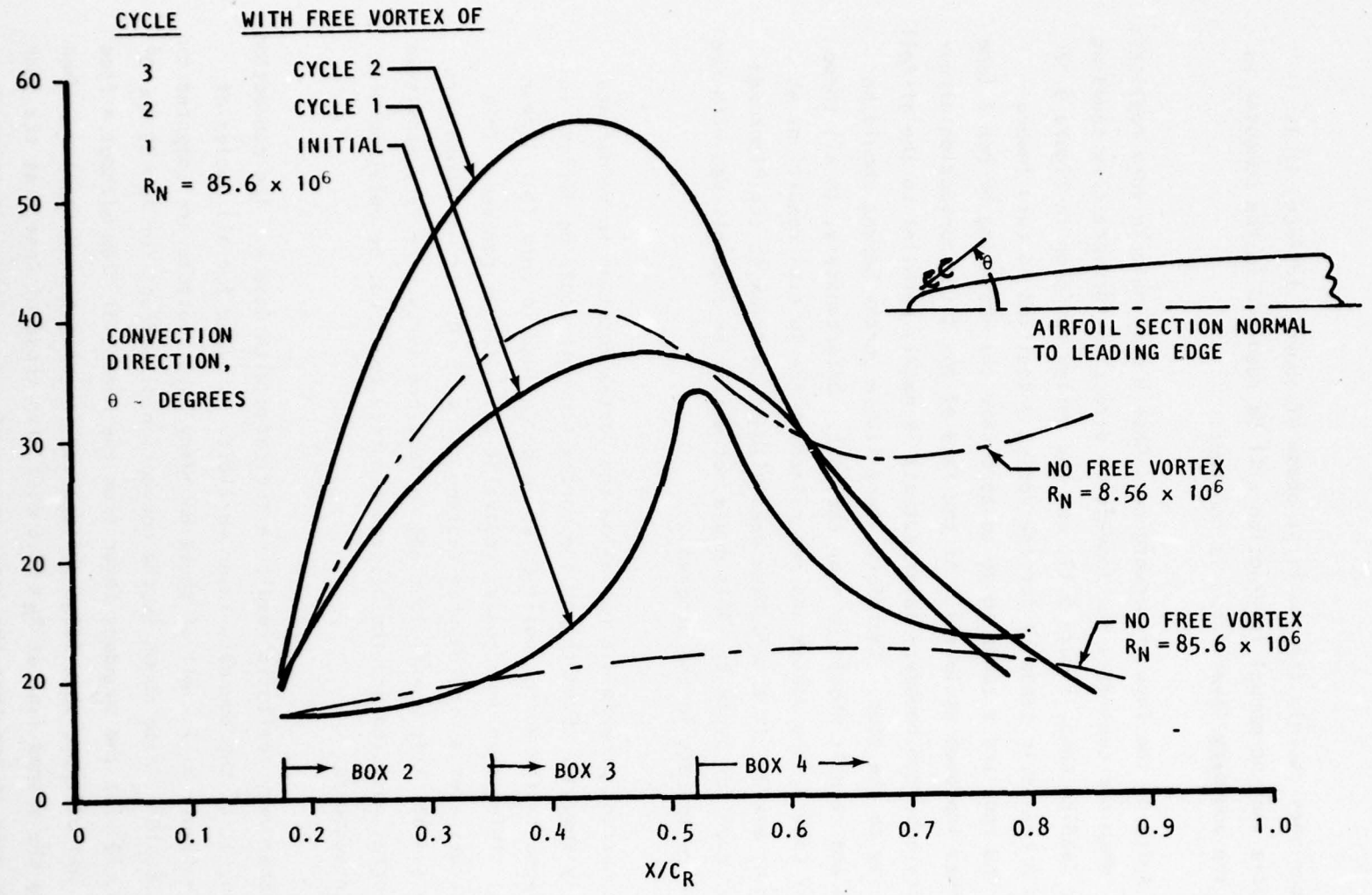

Figure 6.17 Boundary Layer Vorticity Convection Direction

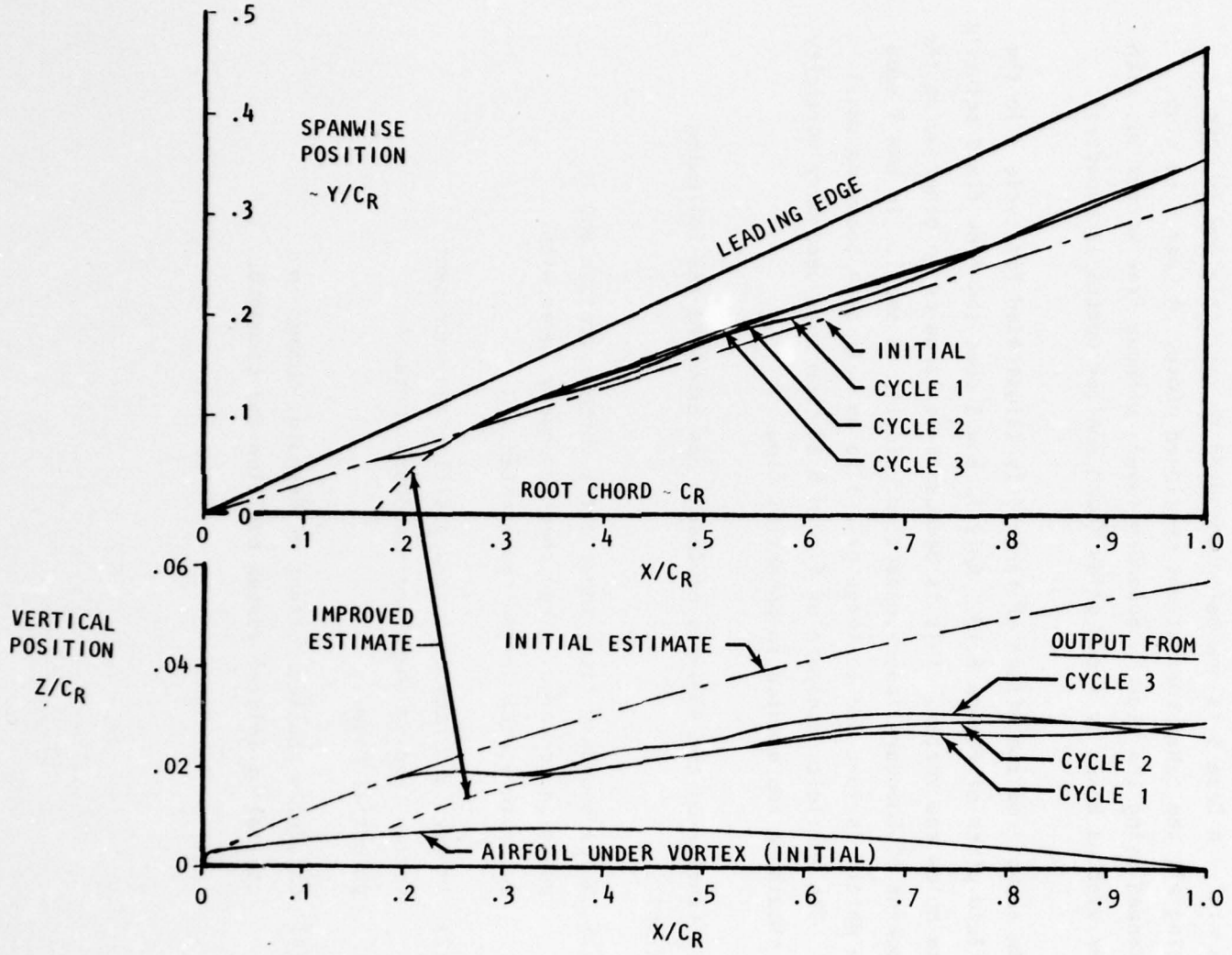

Figure 6.18 Free Vortex Position, Case 4

However, a large θ appears necessary for any significant vortex formation. The realistic conclusion here is that the high R_N of 85.6×10^6 delays large vortex formation to higher angle of attack. On the other hand the data for $R_N = 8.56 \times 10^6$ show that θ is probably high enough for vortex formation at this $\alpha = 14^\circ$. A Case 5 is now being computed to test this low R_N case including all the other corrections mentioned above. A Case 6 is also recommended using the high R_N boundary layer without free vortex but with smaller viscous boxes or finer grids (much smaller vortex is expected).

An example of the effect of large θ is illustrated for cycle 3 in the flow field plots of figure 6.19. Only in box 3 does the flow field actually reverse below the vortex. This is because θ is large or in other words the W component of boundary layer convection velocity is small. In box 4 some of the detail is lost due to large grid size as well as θ becoming small again. The vorticity contours of figure 6.20 show some secondary vorticity which should be represented in potential flow.

In conclusion the analysis of Case 4 has provided the following direction:

(1) Relax boundary layer input until vortex strength and position converge. Then check boundary layer with accurate vortex system represented.

(2) Improve accuracy of vortex position and represent vortex feeding sheet and secondary vortex in potential flow.

(3) Carefully consider effect of Reynolds number in estimating initial vortex position and strength.

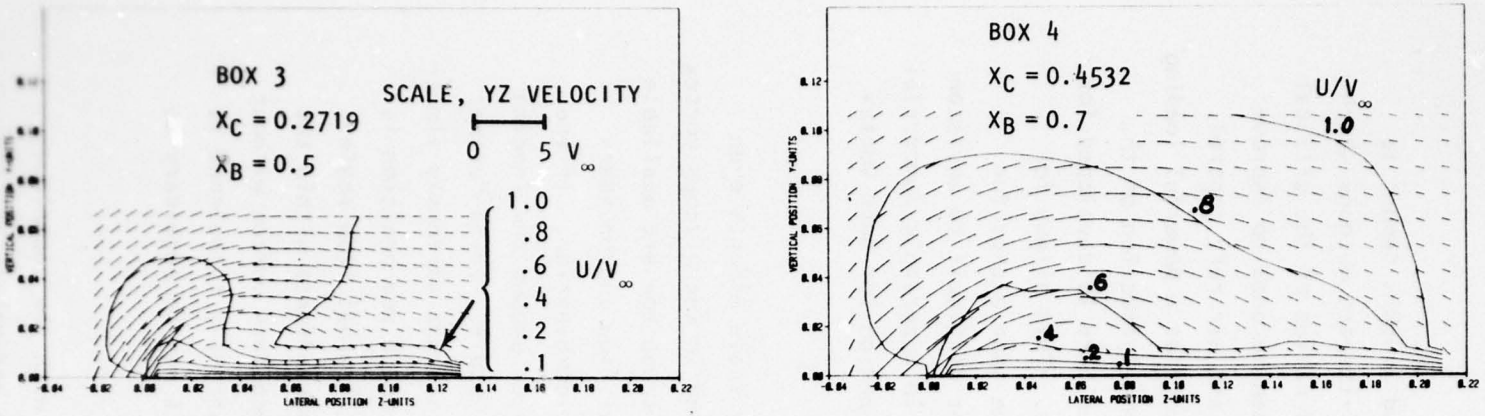

Figure 6.19 Axial and YZ Flow Field Velocities

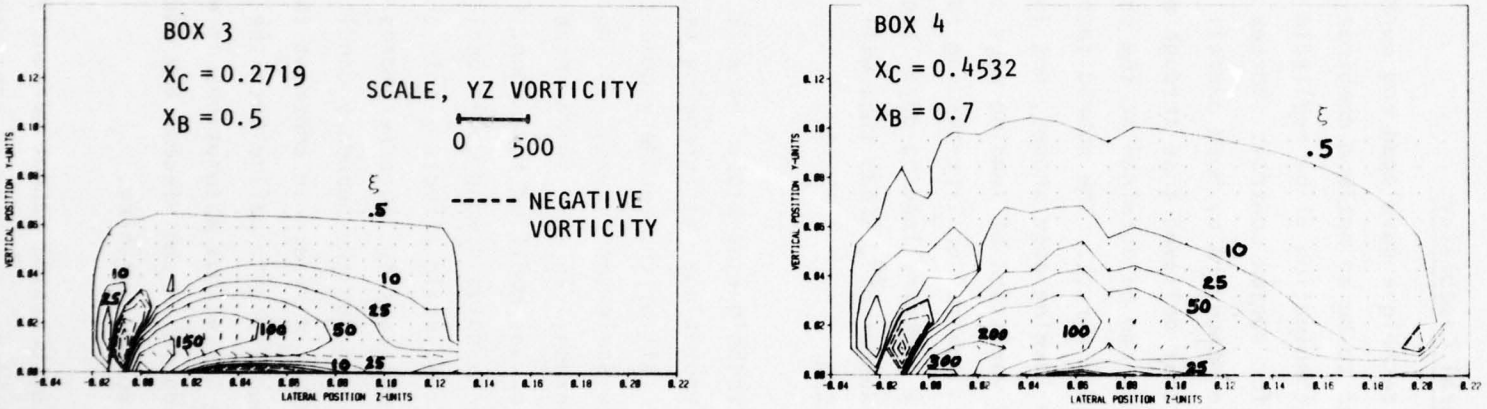

Figure 6.20 Axial and YZ Flow Field Vorticities

7.0 APPLICATIONS

7.1 General Capability

The technique developed and currently discussed in this report is considered to be an optimum combination of state-of-the-art methods which in their combination allow realistic evaluation and design of the critical geometry for vortex control. Vortex control can then be used to improve high angle maneuvers by both overall lift increase and aircraft control. It is further believed that through optimized design that a powerful leading edge vortex can be obtained at the cost of only a small fraction of the leading edge thrust. The hybrid technique discussed here is developed for arbitrary leading edge shapes, not just sharp edges. This allows for optimized variation of leading edge shape across the span either for roll/pitch control or lift-to-drag ratio. It is not difficult to envision a variable geometry leading edge (such as proposed in Supersonic Commercial Aircraft Research[20], SCAR) that will provide optimization for both vortex lift and L/D.

The technique developed here is not limited by scale effects even though computational differencing techniques are used in the viscous vortex analysis. All of the boundary conditions to the viscous box are available from large-scale techniques, i.e. both the potential flow and boundary layer programs. In this sense there is a practical combination. If the viscous box was modified to account for boundary layer around the leading edge, the Reynolds number would be limited to small scale. It is further believed that scale effects within the viscous box are not seriously limiting the application. In other words the vortex strength and position is more dependent on the boundary conditions than the internal flow scale effects or grid size. In contrast though the viscous effects within the box are necessary to define both the primary and secondary vortex without resorting to various assumptions or empiricism. Currently turbulence is not considered in the viscous box analysis, and this may be necessary to consider vortex bursting.

Vortex bursting cannot currently be predicted with the technique discussed here, but there is good prospect that the parameters are available

from the method to use in empirical vortex bursting analyses. One example is the swirl parameter discovered by Wilson[21]. If incipient bursting does not occur in the viscous box before the critical swirl parameter is reached, then the true vortex burst may be predicted by use of Wilson's parameter. Incipient burst is when reverse flow occurs in the direction of the vortex axis. It is here that turbulence may be necessary to realistically delay the incipient burst.

Even though there are several programs involved in the computational procedures of this report, the computer time is relatively small. Currently, it costs $82 or less than 5 minutes of NASA-Ames CDC 7600 computer time to run through one cycle of the procedure; i.e. all programs. It is estimated that, with experience in operating technique, nominally only three cycles will be required to converge the solution with six cycles being the most required. This is 15 to 20 minutes of computer time which is considerably cheaper than the fabrication and modification of wind tunnel models required to get only a part of the information given by the computer method. This is not to say the computer method will eliminate wind tunnel test, but it will allow a more optimized wind tunnel model to be built. An alternate use of the method is to extrapolate results of the wind tunnel tests to large scale. At the same time, synthesis of the various parametric effects will provide knowledge of the details giving a better understanding of the mechanisms and means toward design finesse.

Details of the flow field will be seen even more accurately in the future with further development of the method of this report. For this method is in line to take advantage of the future, rapidly growing, computational techniques. As will be discussed in the recommendations, there are already several improvements that will make the method applicable to more configurations and make it more accurate. It is believed that even now application can currently be made to many configurational problems, and this will improve with update of the method.

Some of the practical applications suggested are as follows:

(1) High Reynolds number optimum spanwise variation in leading edge design to maximize vortex lift to drag ratio for both fighters and supersonic transports.

(2) Optimized variable shape leading edge for high angle-of-attack roll and pitch control.

(3) Canard vortex wing interference design.

(4) Analyses of leading edge vortex effect on wings at high angles of attack in sideslip.

(5) Analyses of empennage surfaces for vortex flow effects while in sideslip.

(6) Design of optimized large leading edge radius for configurations such as the Space Shuttle for optimum vortex lift.

(7) Analyses and optimization of vortex formation on fighter aircraft with swept forward wings and subsequent effects on their empennage.

8.0 CONCLUSIONS

- A theoretical technique has been developed through the hybrid combination of potential and viscous flow models to predict and analyze the flow field and forces due to a discrete leading edge free vortex system. This vortex system can be formed from arbitrary wing planforms with arbitrary edge shapes.

- Some experience has been gained and presented herein of the operating techniques. These techniques are still evolving. Experience has led to improvements of the techniques and to recommendations for further improvement.

- Current applications of the technique have been applied to a 65° delta wing with finite thickness and spanwise variation in leading edge radius. Absolute convergence of the technique has not been obtained, but the current success indicates good probability of convergence. Additional cycles and experience with the operation will provide improved convergence techniques.

- Results to date show that knowledge of rate and direction of leading edge vorticity is an absolute necessity. The overall vortex lift and leading edge thrust are very sensitive to this parameter, and this parameter is highly sensitive to leading edge shape, local angle of attack, Reynolds number and position of transition from laminar to turbulent flow. Turbulent flow separation provides higher vorticity and consequently higher vortex lift.

- The methods used herein do not require any empiricism except probably for future application to vortex burst prediction.

- Currently the methods are best handled with engineering interpretation between some of the steps; however, future operating experience should eliminate this necessity.

9.0 RECOMMENDATIONS FOR FURTHER EFFORT

Recommendations for improvement fall into two categories. One makes significant program changes to current programs and the other makes the current techniques unified as well as conducting applications to determine better operating techniques and make sensitivity studies.

In the first category, six (6) program changes are recommended. These are:

(1) Change coordinate system of viscous box from rectangular to spherical to eliminate jumping in box size and to compute more accurately in a coordinate system natural to vortex growth.

(2) Develop a grid transformation technique with new coordinates to allow more detail near the surface of the wing, improving secondary vortex definition and boundary layer input.

(3) Set the boundary condition on the inboard grid boundary to allow vorticity to exit; i.e. set the gradient of vorticity to zero instead of the vorticity to zero at the exit boundary.

(4) Develop a good representation of vortex feeding sheet for the potential flow model using the results from the viscous flow analysis. This will require a distinction between the vorticity in the discrete vortex and that in the sheet. Defining the velocities in cylindrical coordinates, using the point where both horizontal and vertical components of velocity go to zero as the coordinate center, will help define the vortex core and its circulation. This will also provide the swirl parameter needed for vortex burst analysis.

(5) In the potential flow vortex lattice model, set up panels in the vortex sheet to provide no flow-through conditions.

(6) In the boundary layer program, provide means for automatically transitioning from laminar to turbulent flow using the best physics possible at this time.

In the second category a task should be set up to take advantage of the current programs. The following is recommended:

(1) Combine all programs into one, requiring as little manual interaction as possible. Where manual interaction is required, use computer graphics.

(2) Incorporate grid transformation for rectangular coordinates for same purpose as (2) above.

(3) Conduct sensitivity analysis of box size, Reynolds number, and lower surface attachment line.

(4) Increase number of potential flow model panels to improve pressure distribution around leading edge.

(5) Fabricate model with leading edge radius such as the one in this report and investigate flow field with laser velocimeter to compare results with theory. Test at an angle of attack without vortex burst and one with burst. Analyze with theory for both cases.

(6) Investigate methods for predicting vortex burst using theory and empiricism as discussed in the text.

REFERENCES

1. Matoi, Thomas K.: "On the Development of a Unified Theory for Vortex Flow Phenomena for Aeronautical Applications," Massachusetts Institute of Technology Report, 1 November 1973 - 31 October 1974, for Office of Naval Research, April 14, 1975.

2. Mangler, K. W.; and Smith, J. H. B.: "Calculation of the Flow Past Slender Delta Wings with Leading Edge Separation," RAE Rep. Aero. 2593, May 1957.

3. Polhamus, E. C.: "A Concept of Vortex Lift of Sharp-Edge Delta Wings Based on a Leading Edge Suction Analogy," NASA TN-D-3767, 1966.

4. Lamar, John E.: "Summary of Some Recent Studies of Subsonic Vortex Lift and Parameters Affecting the Leading Edge Vortex Stability," AIAA Paper No. 76-414, July 1976.

5. Weber, James A.; and Guenter, W. B.; Forrester, J. J.; Lu, Paul; and Rubbert, Paul E.: "A Three-Dimensional Solution of Flows Over Wings With Leading Edge Vortex Separation," AIAA Paper 75-866, June 1975.

6. Rao, B. M.; and Nathman, J. K.: "Analytical and Experimental Investigations of Delta Wings in Compressible Flow," Texas A&M University Report TEES-3167-76-01, May 1976.

7. Kandil, O. A.; Mook, D. F.; and Nayfeh, A. H.: "New Convergence Criteria for the Vortex Lattice Models of the Leading Edge Separation," *Vortex-Lattice Workshop*, NASA SP-405, May 1976.

8. Hall, G. T.; Shamroth, S. J.; McDonald, H.; and Briley, W. R.: "The Inviscid Pressure Field on the Tip of a Semi-Infinite Wing and Its Application to the Formation of a Tip Vortex," NASA Contractor Report, NASA CR-2748, October 1976.

9. Scruggs, R. M.; and Dixon, C. J.: "Theoretical and Experimental Investigations of a Jet Parallel to Wing in Cross Flow," Final Report, Office of Naval Research Contract, Lockheed-Georgia Engineering Report LG75ER-0028, April 30, 1975.

10. Scruggs, R. M.; and Dixon, C. J.: "Vortex/Jet/Wing Viscous Interaction Theory and Analysis," Office of Naval Research Report ONR-CR-215-233-2, February 2, 1976.

11. Dixon, C. J.; and Scruggs, R. M.: "Further Development of a Viscous Vortex/Wing Interaction Program," Office of Naval Research Report ONR-CR215-233-3, June 1977.

12. Henderson, W. P.: "Effects of Wing Leading Edge Radius and Reynolds Number on Longitudinal Aerodynamic Characteristics of Highly Swept Wing-Body Configurations at Subsonic Speeds," Langley Research Center NASA TN-D-8361, December 31, 1976.

13. Hess, John L.: "Calculation of Potential Flow About Arbitrary Three-Dimensional Lifting Bodies," Technical Report for Naval Air Systems Command, McDonnell Douglas Aircraft Corp. Report No. MDCJ5679-01, October 1972.

14. Nash, J. F.: and Tseng, R. R.: "The Three-Dimensional Turbulent Boundary on an Infinite Yawed Wing," *Aeronautical Quarterly*, 1971.

15. Nash, J. F.; and Patel, V. C.: *Three-Dimensional Turbulent Boundary Layers*, SBC Technical Books, 1972.

16. Compsty, N. A.; and Head, M. R.: "The Calculation of Three-Dimensional Turbulent Boundary Layers. Part III: Comparison of Attachment Line Calculations with Experiment," *Aeronautical Quarterly*, 20, p. 99, 1969.

17. Dixon, C. J.: "Theoretical and Experimental Investigations of Vortex Lift Control by Spanwise Blowing," Office of Naval Research Contract Report, Lockheed-Georgia Engineering Report, Vol. I, LG73ER0169, September 1973.

18. Roache, P. J.: *Computational Fluid Dynamics*, Hermosa Publishers, Albuquerque, New Mexico, 1972.

19. Sampath, S.; and Hackett, J. E.: "Application of the 'Vorticity Box' Program to Vortex Flows: A Study of Numerical Errors," Lockheed-Georgia Report LG77ER0233, December 1977.

20. Boeing Airplane Company, "Supersonic Cruise Aircraft Noise Sensitivity and Low-Speed Performance Improvement Studies," NASA CR-145286-1, July 1978.

21. Wilson, J. D.: "Calculation of Vortex Breakdown Locations for Flow Over Delta Wings," AIAA *Journal of Aircraft*, Vol. 14, No. 10, October 1977.

DISTRIBUTION LIST

Office of Naval Research
800 N. Quincy St.
Arlington, VA 22217
- ONR 211 — 4
- ONR 430B — 1

Office of Naval Research Branch Office
1030 E. Green St.
Pasadena, CA 91106 — 1

Office of Naval Research Branch Office
Bldg. 114 Section D
666 Summer St.
Boston, MA 02210 — 1

Office of Naval Research Branch Office
536 South Clark St.
Chicago, IL 60605 — 1

Naval Research Laboratory
Washington, DC 20375
- Code 2627 — 1
- Code 2629 — 1

Defense Documentation Center
Bldg. 5 Cameron Station
Alexandria, VA 22314 — 12

Naval Air Systems Command
Washington, DC 20361
- AIR 320D (Mr. R. Siewert) — 1

Naval Air Development Center
Warminster, PA 18974
- Code 6053 (Dr. K. T. Yen) — 2

David Taylor Naval Ship Research and Development Center
Bethesda, MD 20084
- Code 16 (Dr. H. Chaplin) — 1
- Code 1843 (Ms. J. Schot) — 1
- Code 522.3 Aero Library — 1

U. S. Naval Postgraduate School
Monterey, CA 93940
- Dept. of Aeronautics (Code 57) — 1
- Library — 1

Superintendent
U. S. Naval Academy
Annapolis, MD 21402 — 1

NASA Ames Research Center
Moffett Field, CA 94035
- FAE Branch — 1
- FAR Branch — 1

NASA Langley Research Center
Hampton, VA 23665
- Mr. R. Margason — 1
- Dr. J. Cambell — 1

Wright Patterson Air Force Base
Dayton, OH 45433
- Aero & Airframe Branch (Dr. T. Weeks) — 1

Air Force Office of Scientific Research
Bolling AFB, DC 20332
- Code NA (Dr. J. Wilson) — 1

Defense Advanced Research Projects Agency
1400 Wilson Boulevard
Arlington, VA 22209
- Mr. R. Moore — 1

Lockheed Missiles & Space Co., Inc.
Huntsville Research & Engineering Center
P. O. Box 1103
Huntsville, AL 35807
- Mr. A. Zalay — 1

Nielsen Engineering & Research, Inc.
510 Clyde Avenue
Mountain View, CA 94043 — 1

McDonnell Douglas Aircraft Company
P. O. Box 516
St. Louis, MO 63166
- Aerodynamics (Dr. D. Kotansky) — 1

Vought Corporation
Advanced Technology Center, Inc.
P. O. Box 6144
Dallas, TX 75222
Dr. Gary Hough 1

Grumman Aerospace Corporation
Bethpage, NY 11714
Research Dept. (Dr. R. Melnik) 1

Rockwell International
Columbus Aircraft Division
Columbus, OH 43216
Research Dept. (Dr. P. Bevilaqua) 1

University of Southern California
Dept. of Aerospace Engineering
University Park
Los Angeles, CA 90007
Prof. John Laufer 1

Virginia Polytechnic Institute
Dept. of Engr. Sciences & Mechanics
Blacksburg, VA 24061 1

University of Maryland
Dept. of Aerospace Engr.
College Park, MD 20742
Dr. J. D. Anderson, Jr. 1

United Aircraft Corporation
Research Laboratories
Silver Lane
East Hartford, CT 06108
Dr. M. Werle 1

Polytechnic Institute of New York
Long Island Center
Dept. of Aero Engr. and Applied
Mechanics
Route 110
Farmingdale, NY 11735
Prof. S. Rubin 1

Scientific Research Associates, Inc.
P. O. Box 498
Glastonbury, CT 06033
Dr. H. McDonald 1

National Science Foundation
Engineering Division
1800 G. St., NW
Washington, DC 20550 1

Army Research Office
P. O. Box 12211
Research Triangle Park, NC 27709 1